UNIVERSITY OF UDINE

DEPARTMENT OF MEDICAL AND BIOLOGICAL SCIENCE

PhD COURSE IN CLINICAL SCIENCE AND TECHNOLOGY
XXVII CICLE

PhD THESIS

MULTIMERIN2:
a key regulator of tumor angiogenesis and vascular homeostasis

PhD student:

Rosanna Pellicani

TUTOR:

Prof. Francesco Curcio

SUPERVISOR:

Dott. Maurizio Mongiat

PhD Coordinator:

Prof. Giuseppe Damante

ACADEMIC YEAR

2014/2015

TABLE OF CONTENTS

1. ABSTRACT

Angiogenesis, the formation of new blood vasculature from pre-existing vessels, is a hallmark of cancer. The extracellular matrix (ECM) molecule, MULTIMERIN2 (MMRN2), is specifically deposited along the vasculature in tight juxtaposition with endothelial cells (ECs). We have previously demonstrated that the glycoprotein halts ECs' motility and impairs tumor angiogenesis through the interaction with VEGF-A_{165}, leading to the down-regulation of VEGF-A/VEGFR2 signaling axis. In this study, we identified the region of the MMRN2 responsible for the binding, demonstrating that the interaction involves the carbohydrate chains. We have also found that MMRN2 interacts with other VEGF-A isoforms and VEGF family members suggesting that the molecule may function as a reservoir for different cytokines. Moreover, we demonstrated that the anti-migratory function of the molecule hinges on a reduced VEGFR2 phosphorylation at both Y1175 and Y1214, which leads to the down-modulation of SAPK2/p38 activation. Furthermore, we found that MMRN2 impaired VEGFR2 function by reducing its availability at the ECs' plasma membrane.

Through *in vitro* and *in vivo* tests we demonstrated the angiostatic role of MMRN2 and its active fragment and, as a consequence, the over-expression of the molecule or its active deletion mutant by cancer cells led to a dramatic reduction of tumor growth.

Given its strategic localization, we have recently hypothesized that MMRN2 may represent a homeostatic molecule buffering the angiogenic stimuli and maintaining the endothelium quiescent. In line with this hypothesis MMRN2 is deposited over time during vessel maturation and the co-culture of ECs with pericytes boosts its secretion and organization. In addition, we have demonstrated that MMRN2 represents an adhesion substrate for pericytes and may be required for their recruitment, since pericyte coverage of the MMRN2 knockout retinal vessels is strongly impaired. We also found that the down-modulation of MMRN2 leads to an increased vascular permeability associated with an impaired expression of the tight junction-associated molecules occludin and ZO-1. Accordingly, preliminary data show that the MMRN2 knockout mice displayed an increased vascular leakage. Taken together these results pinpoint MMRN2 as a key angiostatic molecule that can be regarded as a promising novel tool for the development of new anti-angiogenic drugs.

2. ABBREVIATIONS

Ad MMRN2: Adenovirus MMRN2

AJ: Adherens Junctions

BM: Basement Membrane

CLDN: Claudins

Coll I: Type I Collagen

EC: Endothelial Cell

ECM: Extracellular Matrix

FBS: Fetal Bovine Serum

FGF: Fibroblast Growth Factor

HUVEC: Human Umbilical Vein Endothelial Cell

HBVP: Human Brain Vascular Pericytes

JAM: Junctional adhesion molecule-A

MMRN2: MULTIMERIN2

MMPs: Matrix Metalloproteases

PBS: Phosphate Buffered Saline

PDGF: placental-derived growth factor

siRNA: Small Interfering RNA

TGF-β: Trasforming Growth Factor-beta

TJ: Tight Junctions

TUNEL: TdT-mediated dUTP Nick End Labeling

VE-cadherin: Vascular Endothelial-cadherin

VEGF: Vascular Endothelial Growth Factor

VEGFR2: Vascular Endothelial Growth Factor Receptor

ZO: Zona occludens

3. INTRODUCTION

3.1 Angiogenesis.

Blood vessel formation is regulated by two fundamental processes termed vasculogenesis and angiogenesis (Carmeliet P., 2000; Risau W., 1997; Risau and Flamme., 1995). Vasculogenesis is defined as the differentiation of precursor cells (angioblasts) into endothelial cells (ECs) and the *de novo* formation of a primitive vascular network. On the contrary, angiogenesis is the formation of new capillaries from pre-existing vasculature. In the embryo, blood vessels form through both vasculogenesis and angiogenesis. Whereas, in the adult, the angiogenetic process occurs only in particular conditions such as wound healing, menstrual cycle as well as in various ischemic and inflammatory diseases to allow the maintenance of physiological homeostasis (Carmeliet P., 2003).
Blood vessels are a complex network of tubes that transport oxygenated blood and nutrient throughout the body and are composed of different interacting cell types. In particular, ECs line the inner side of the vessel wall, and mural perivascular cells which envelop the surface of the vascular tube and include pericytes and vascular smooth muscle cells. Pericytes have an important role in maintaining vascular homeostasis and when vessels lose their coverage they become hemorrhagic and hyperdilated. This condition can lead to edema, diabetic retinopathy, and even embryonic lethality (Bergers G. and Song S.,2005).
Normal angiogenesis relies on a proper interaction between ECs, pericytes and surrounding cells and their association with extracellular matrix (ECM) components, including the constituents of the vascular basement membrane (BM). The BM divides the ECs from the surrounding connective tissue and is mostly composed of laminins, collagen and proteoglycans (Lebleu V.L. et al., 2007).

The angiogenic process takes place through the engagement of multiple steps (Fig. 1):

1) Production of angiogenic growth factors (such as vascular endothelial growth factor, VEGF-A) and the binding to their receptors on the ECs surface that leads to the activation of specific signaling pathways;

2) Release of proteases, including matrix metalloproteases (MMPs), by ECs which lead to ECM degradation and support and guidance ECs migration;

3) Proliferation of ECs that leads the formation of capillary sprouts;

4) Migration of ECs towards the angiogenic stimulus;

5) Tube formation with an encased lumen sealed by tight cell-cell junctions, synthesis of BM proteins and assembly of a new BM;

6) Anastomosis, the process through which the capillaries emanating from the arterioles and the venules come together and allow the flow of blood within the mature vessel.

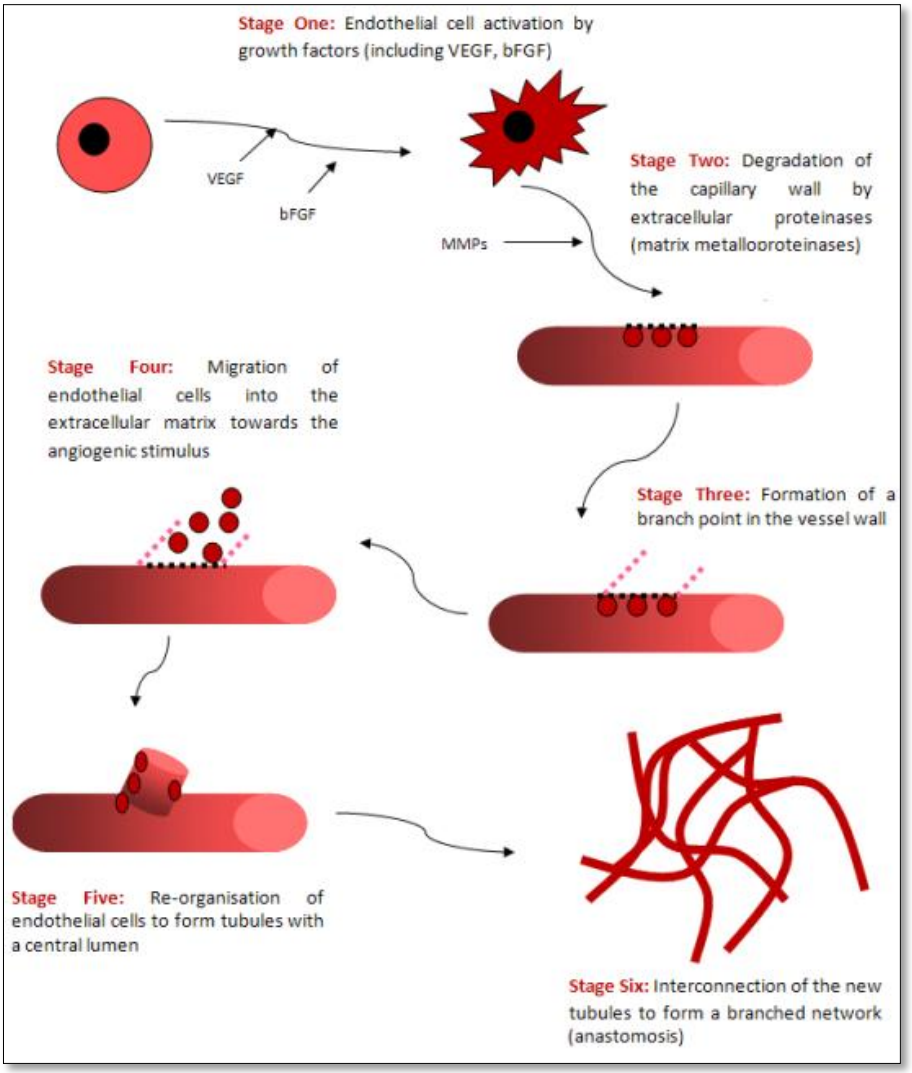

Fig. 1: Scheme of the sequential steps characterizing angiogenesis. Six critical steps occuring during this tightly regulated process have been identified and described.

3.2 The endothelial barrier.

The endothelium, a tight monolayer of ECs, acts as a dynamic barrier that allows the passage of fluids, electrolytes and proteins from the blood into the adjacent tissues. The integrity of this barrier is crucial for the maintainance of the circulatory homeostasis and the physiological functions of the various organs. The passage of macromolecules, fluids and cells through this barrier can occur via either the transcellular or the paracellular pathways (Gavard J., 2009). The first pathway is responsible for the transport of small molecules (inferior to 3 nm), such as albumin, which involves a system of trafficking vesicles, called vesicular vacuolar organelles. On the contrary, cells and molecules larger than 3nm are transported through the paracellular pathway, which occurs for instance during the trans-endothelial migration of leukocytes and metastatic cells. The paracellular permeability is dependent on a coordinated aperture and closure of endothelial cell-cell junctions.

In the endothelium, the junctional complexes comprise adherens junctions (AJ), tight junctions (TJ) and gap junctions (Fig. 2). Gap junctions, formed of connexins, allow the passage of water and ions but they are not involved in the regulation of the vascular barrier. AJs are found in all microvascular beds, and are the most ubiquitous type of endothelial cell–cell junctions. Among different AJ molecules, one of the most important is the vascular endothelial cadherin (VE-cadherin), which is exclusively expressed by ECs (Dejana E., 2004). The deletion of the VE-cadherin gene in mice leads to early embryonic lethality due to substantial vascular defects, whereas loss of its function induces hyperpermeability in adult mice (Carmeliet P. et al., 1999; Crosby CV. et al., 2005).
TJ consist of several transmembrane or membrane-associated proteins including the membrane spanning claudins (CLDN), occludin (OCLN) and the JAM family of junctional adhesion molecules (Dejana E., 2004). OCLN and CLDN are integral membrane proteins, each with four transmembrane domains and two extracellular loops. OCLN is expressed at high levels, with a continuous distribution along the ECs of the brain and at much lower levels and with a discontinuous pattern in ECs of other tissues (Hirase T. et al., 1997).
The TJ are connected to the actin cytoskeleton via adaptor proteins such as ZO-1, ZO-2, ZO-3, cingulin, AF6 or 7H6 (Beese M. et al., 2010).

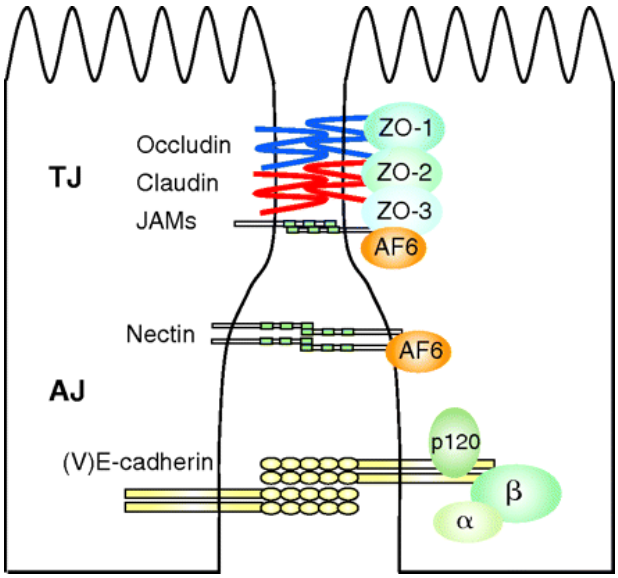

Fig. 2: Schematic overview of the adherens and tight junctions. α, α-catenin; AF6, afadin/AF6; AJ, adherens junctions; β, β-catenin; JAMs, junctional adhesion molecules; p120, p120catenin; TJ, tight junction; ZO, zona occludens.

The endothelium and its junctions play a critical role in regulating vascular functions during both pathological and physiological processes. Dysregulation of cell junctions and a significant increase in vascular permeability can lead to pathological situations including inflammation, trauma, ischemia/reperfusion injury, thrombosis, sclerosis (Yuan SY. And Rigor RR., 2010).

Vascular permeability involves the coordinated regulation of multiple signaling pathways in the ECs (Aghajanian A. et al., 2008), thus, the identification of the most mechanisms regulating this process open the possibility to develop new targets for therapeutic treatment or new prognostic markers in many pathological disease where vascular permeability is adversely affected.

3.3 Vascular endothelial growth factors.

Among the many factors implicated in angiogenesis, VEGF has been identified as one of the most important players in vascular EC growth, survival, and permeability. The VEGF family comprises seven members including placental-derived growth factor (PDGF), VEGF-A, VEGF-B, VEGF-C, VEGF-D, VEGF-E, VEGF-F, encoded by multiple exons that can give rise to different isoforms after alternative splicing. The inclusion or exclusion of exons can have important consequences in the regulation of angiogenesis, since the variants are characterized by different solubility and affinity for receptor binding (Sullivan and Brekken., 2010).
In particular, VEGF-A can be generated in four major homodimeric isoforms $VEGF_{121}$, $VEGF_{165}$, $VEGF_{189}$, and $VEGF_{206}$. All these isoforms, except VEGF121, bind to heparin and therefore are in close association with the ECM. Also VEGF-B is present in two isoforms constituted by 167 and 186 amino acid residues. Little is known about alternative splicing of human VEGF-C and VEGF-D, although multiple isoforms of mouse VEGF-D have been described (Baldwin ME. Et al., 2001).
VEGF is produced by several cell types, such as tumor cells (Aonuma M. et al., 1999), muscle (Bryan BA. et al., 2008) and neuronal cells (Jin et al., 2006), but its actions is mainly associated to ECs.
Following a hypoxic stimulus, VEGF binds to VEGFR-1 (Flt-1), VEGFR-2 (Flk1/KDR), and VEGFR-3 (Flt4), three membrane tyrosine kinase receptors mainly expressed by blood vessel ECs and lymphatic ECs (Koch S. and Claesson-Welsh L. et al., 2012). Although with different biological activities, all VEGFRs play an important role in angiogenesis. In fact, the knockout of VEGFR-1, VEGFR-2, and VEGFR-3 leads to embryonic lethality in mice as a result of severe vascular defects (Goishi K. et al., 2004). Interestingly, the VEGFR2 receptor, characterized by a strong kinase activity, is the predominant mediator of VEGF-induced angiogenic signaling, despite having a lower affinity for VEGF if compared to VEGFR1. Probably due to its strong activity, VEGFR-2 is also the major responsible for hyperpermeability induced by VEGF. Some evidences have been generated indicating that VEGFR-1 also plays a role in endothelial permeability but the contribution of the receptor appears to be minor compared to that of VEGFR2.
Once VEGF binds VEGFR2, it induces receptor homo- or heterodimerization and its auto-phosphorylation. The major phosphorylation sites on VEGFR2 occur on tyrosines 1175 and 1214 inducing the activation of signaling cascades through PI3K, AKT, PLCγ, p38 MAPK and p42/44 MAPK, which in turn regulate EC survival, migration, proliferation and vascular permeability (Takahashi T. et al., 2001; Lamalice L. et al., 2004) (Fig. 4).

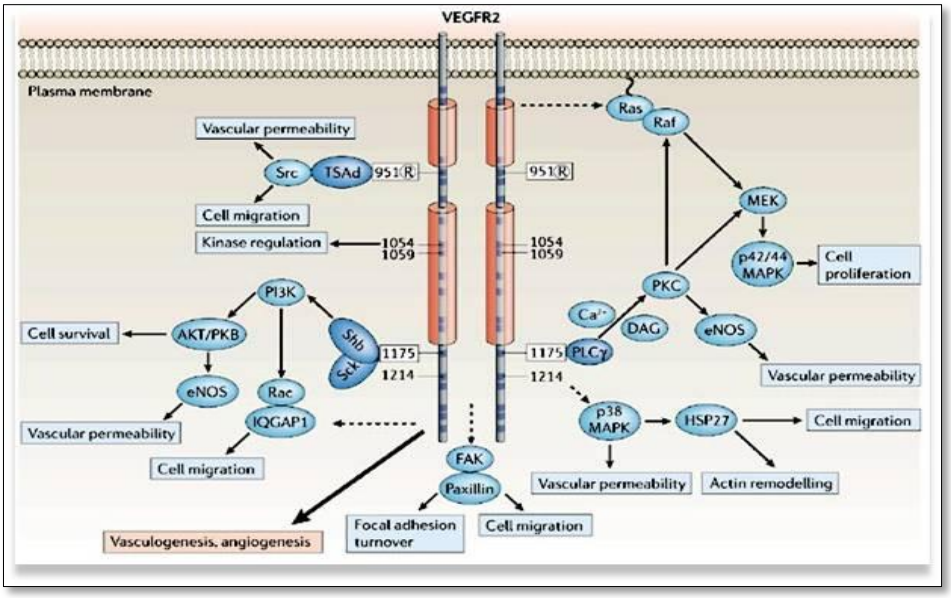

Fig 4: VEGFR2 phosphorylation sites and signal transduction. Schematic representation of the intracellular domains of dimerized and activated VEGFR2; the different tyrosine-phosphorylation sites that are indicated by the amino acid residue's numbers. The position of the tyrosine residues within the receptor are indicated by dark blue squares. The signaling molecules (dark blue ovals) binding to specific phosphorylation sites (boxed numbers) initiate signaling cascades (light blue ovals), which leads to the establishment of specific biological responses (pale blue boxes). Dashed arrows indicate that the signal initiation is not certain. The biological responses are highlighted by pink boxes (Olsson A.K. et al., 2006).

3.4 Tumor angiogenesis.

Angiogenesis is governed by a finely tuned balance between pro-angiogenic factors, that induce the formation of blood vessels, and anti-angiogenic-factors, which inhibit the process. Once this balance is jeopardized it leads to the formation of structurally defective vessels. This occurs for instance during tumor formation, where the over-production of growth factors leads to the development of numerous dysmorphic vessels that allow tumor growth and metastasis. Tumor formation begins with an avascular mass with an intrinsic tumorigenic potential that alone is not sufficient to support tumor activation (Papetti M. et al., 2002).
These small lesions, of not more than 1-2 mm in diameter linger in a steady dormant state (Folkman J., 1971) and only few became exponentially growing vascularized tumors (Fig. 5).
The accumulation of genetic alterations empowers some neoplastic cells with the ability to secrete large amounts of pro-angiogenic factors such as VEGF and/or suppress the expression of anti-angiogenic molecules like transforming growth factor-beta, TGF-β. In turn, this leads to a dismantled local balance between activators and inhibitors of angiogenesis and the pro-agiogenic factors take over giving rise to the process called the "angiogenic switch" (Hanahan D. et al., 1996). Following secretion, the pro-angiogenic factors diffuse through the tissue and activate the ECs adjacent to the tumor.

These cells lose the tight contacts with neighbouring cells (Papetti M.et al., 2002) and secrete proteolytic enzymes and proteases to degrade BM and ECM, allowing their migration into the perivascular space towards angiogenic stimuli (Pepper M.S., 2001). Following extravasation, the ECs continue to secrete proteolytic enzymes, which also degrade the ECM. This is necessary to create a pathway along which the cells can move and also allows the release of growth factors that are normally sequestered by the matrix, thus further boosting the angiogenic signals (Hirschi K. K. et al., 1996). ECs continue to move forming small sprouts which elongate through the recruitment of additional ECs from the parent vessel. These sprouts take the form of solid strands of cells and ECs subsequently form a central lumen, thereby creating the necessary structure for a new blood vessel. Differently from normal vasculature, which is characterized by a hierarchical organization into arteries, arterioles, capillaries, venules and veins, the vessels associated with solid tumors are characterized by a number of prominent abnormalities. Frequent aberrations are the presence of dilated blood vessels, vessels with areas containing absent or abnormal BM, vessels having extreme tortuosities, the lack of supporting perivascular cellular elements such as pericytes, or abnormalities in the pericyte population and excessive vascular leakiness (Carmeliet P. et al., 1996). Consequently, blood flow and perfusion within tumors can be highly altered with some areas deprivated of oxygen and nutrients leading to the formation of hypoxic ischemic regions and to tumor cell necrosis (Nagy JA. et al., 2009).

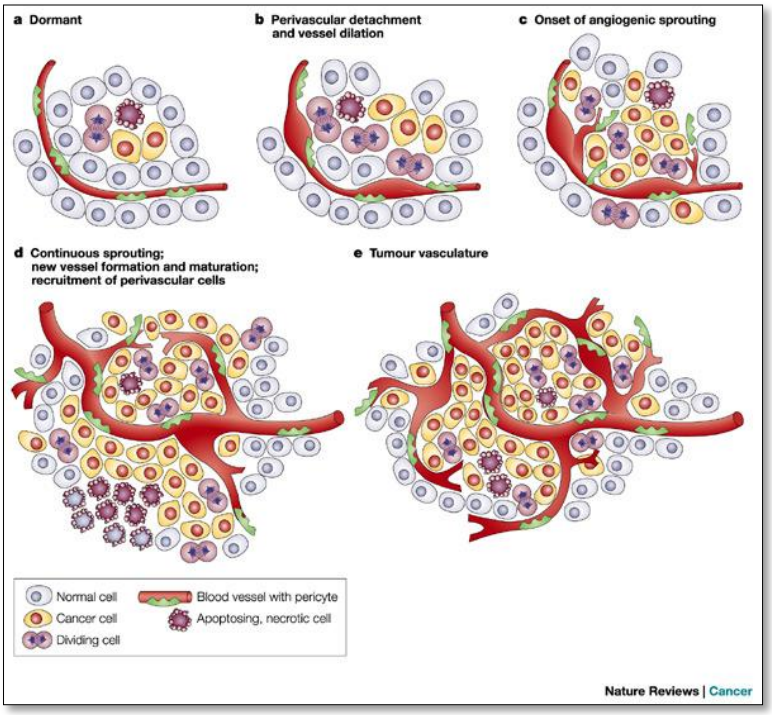

Fig. 5: The classical angiogenic switch. Schematic representation of the different processes occurring in the tumor-progression pathway (Bergers G. and Benjamin LE., 2003). The tumoral mass starts growing as an avascular dormant nodule (a) until it reaches a steady-state level where the number of proliferating cells is balanced by those undergoing apoptosis. The angiogenic switch, necessary to ensure exponential tumor growth, begins with perivascular detachment and vessel dilation (b), followed by angiogenic sprouting (c), new vessel formation and maturation, and the recruitment of perivascular cells (d). Blood-vessel formation will continue as long as the tumour grows (e).

VEGF-A not only plays a central role in normal angiogenesis but also in tumor-associated angiogenesis. The growth factor and its receptor VEGFR2 are in fact upregulated in many cancers including breast cancer (Kurebayashi J. et al., 1999), colon cancer (Shaheen RM. et al., 1999), hepatoma (Yoshiji H. et al., 1999), gastric cancer (Kitamura M. et al., 1998) and prostate cancer (Balbay MD. et al., 1999). In addition, a high expression of VEGF correlates with invasiveness, vascular density, appearance of metastasis, and poor prognosis (Seo Y. et al., 2000). Due to its pleiotropic effects, several strategies to target VEGF or its receptor have been attempted and are currently under development. These include monoclonal antibodies directed against VEGF or VEGFR, soluble VEGFR/VEGFR hybrids, and a variety of small-molecule VEGFR tyrosine kinase inhibitors. Although these agents have often been proved efficacious in pre-clinical experimental settings, results in human cancer have been less impressive, probably due to the heterogeneity of the tumor vasculature (Ebos JM. et al., 2009; Carmeliet P. and Jain RK., 2011; Cascone T. and Heymach JV., 2012; Ferrara N., 2005). An emerging alternative to ameliorate the therapeutic outcome, avoid resistance and improve chemotherapic and radiotherapic treatments is possibility to readdress the aberrant tortuous and leaky vessels associated with tumours towards a normalized more efficient vasculature (Sorensen AG. et al., 2012; Emblem KE. et al., 2013; Jain RK. 2014; Wong PP. et al., 2015).

3.5 The extracellular matrix.

The extracellular matrix (ECM) is an intricate network of non-cellular components, made by proteins and water-absorbing polysaccharides in which the cells of the microenvironment are embedded (Bissell M.J. et al., 2005). It is present in all tissues and organs and provides not only physical scaffolding for the cellular components, but also activates the biochemical and mechanical signals required for tissue morphogenesis, differentiation and homeostasis. These effects are further amplified by the intrinsic property of the ECM molecules to function as reservoirs of growth factors, cytokines, matrix metalloproteinases and processing enzymes (Sternlicht M.D.et al., 2001). The relative availability of these elements increases once the ECM rearranges and it is enzymatically processed during wound healing or tumor progression. The ECM is a highly dynamic structure undergoing continuous remodelling, which consists in the deposition, degradation, and modification of its components. Two main classes of macromolecules compose the ECM: glycosaminoglycans (GAGs) and fibrous proteins which include collagen, elastin, fibronectin, and laminin. These proteins are majorly produced by fibroblasts as precursor molecules and then are incorporated into the ECM in accordance with the needs of the tissues.

Collagen is the most abundant protein in the human body, it provides tensile strength, regulates cell adhesion, supports chemotaxis and migration, and directs tissue development (Rozario T. and DeSimone DW., 2010). Collagen is associated with elastin, a flexible protein that allows tissues to return to their original shape following a stretch. Fibronectin, another fibrous protein, is an important substrate for cell migration but it was also demonstrated to regulate cell division.

The importance of ECM proteins is highlighted by the fact that a wide variety of human syndromes are caused by mutations in the genes encoding for this type of proteins (Jarvelainen et al., 2009).

Not only the fibrous ECM proteins play a structural and also functional role in regulating cell function, but also some members have been demonstrated to exert an active part in the regulation of angiogenesis. In particular, Collagen IV (Mammoto T. et al., 2013), and laminin (Simon-Assmann P. et al., 2011), provide structural support for ECs and blood vessel formation thanks to the adhesive interactions occurring with the EC surface integrin receptors. Thus, through the engagement of the integrins and also by different mechanisms, the ECM affects many fundamental aspects of the EC biology, including proliferation, migration, morphogenesis, survival, as well as blood vessel development and stabilization (Ingber DE. Folkman J., 1989; Neve A. et al., 2014; Senger DR, Davis GE., 2011; Cheresh DA, Stupack DG., 2008). Other ECM molecules that have been shown to affect angiogenesis are fibronectin (Yi M. Ruoslahti E., 2001), vitronectin (Li R. et al., 2014), , thrombospondins (Lawler PR, Lawler J., 2012), SPARC (Jendraschak E, Helene Sage E., 1996), perlecan (Aviezer D. et al., 1994) and decorin (Jarvelainen H. et al., 2015). To further complicate this scenario, ECM proteolytic fragments can also affect angiogenesis, often exerting opposite effects compared to the intact molecule of origin. The degradation and liberation of matrix fragments is regulated by specific proteinases produced by ECs following angiogenic stimulus, which include the plasminogen activator (PA)/plasmin system and matrix metalloproteinases (MMPs). The first is an enzymatic cascade involved in the control of fibrin degradation, matrix turnover, and cell invasion. On the contrary, MMPs belonging to the family of zinc endopeptidases, can exist in both soluble and membrane-bound (MT-MMPs) forms. These proteases are produced by many cells, including epithelial cells, fibroblasts, inflammatory cells, and ECs. At least, five MMPs have a role in angiogenesis: MMP1, MMP2, MMP3, MMP7, and MMP9, often upregulated in ECs in physiological and pathological conditions (Davis GE. et al., 2001).

3.6 The EMILIN protein family.

EMILINs are a family of ECM glycoproteins characterized by the presence of a cysteine-rich EMI domain at the N-terminus. Moreover, most of these members also display a gC1q-like domain at the C-terminus (Doliana R. et al., 2000; Mongiat M. et al., 2000). These glycoproteins can be clustered into three groups:

- The first group (Fig. 6) includes EMILIN1 (Doliana R. et al., 2000), EMILIN2 (Doliana R. et al., 2000), MULTIMERIN1 (Hayward C.P. et al., 1991) and MULTIMERIN2 (Christian S. et al.,2001)

- The second group is composed by only one gene named EMILIN3. The protein has a structure similar to that of the previous group except for the lack of the gC1q domain (Leimeister C. et al., 2002). As recently reported, the protein is able to function as an extracellular regulator of the activity of TGF-β ligands (Schiavinato A. et al., 2012).
- The last group includes two genes, Emu1 and Emu2, which unlike the other groups, present only the EMI domain at the N-terminus. These two proteins display a completely different structure compared to the other members given that most of their sequence is collagenous (Leimeister C. et al., 2002)

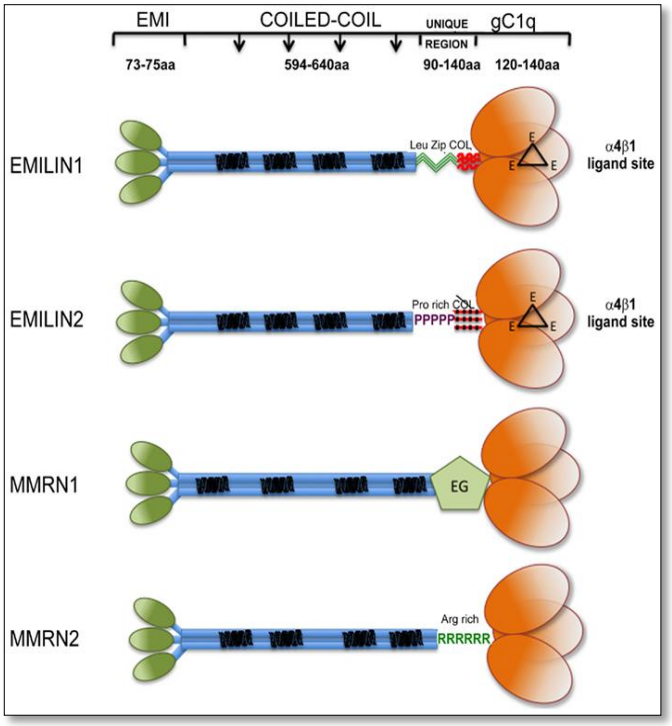

Fig. 6: Graphical representation of EMILIN/Multimerin family members.(EMI) EMI domain; Coiled-coil region; (C1q) gC1q-like domain; (PR) prolin-rich domain; (RR) arginine-rich domain; (EG) region with partial similarity with EGF domain (Colombatti A. et al., 2011).

3.6.1 EMILIN1.

EMILIN1, the archetype protein of the family, was originally identified during the isolation of elastic-specific glycoproteins. EMILIN1, a protein of 115 kDa is specifically localized at the interface between the amorphous elastin surface and microfibrils, hence the acronym (Elastin Microfibril Interface Located proteIN) (Bressan G. et al., 1993). The protein, it is highly expressed at the level of large blood vessel wall and in the connective tissue of a wide array of organs (Colombatti A. et al., 1985). During mouse development, EMILIN1 mRNA is expressed along the blood vessels and perineural mesenchyme (Braghetta P. et al., 2002). In addition, intense labeling is identified in the mesenchyme of many organs including lung and liver and in different mesenchymal condensations such as limb bud and branchial arches. At late gestation stages EMILIN1 staining is widely distributed in the interstitial connective tissue and in smooth muscle cell-rich tissues. After birth, the EMILIN1 mRNA expression levels decline with the age increase. EMILIN1 displays different functions:

- It has adhesive and migratory properties for different cell types. It is a ligand for the α4β1 integrin and the interaction occurs through the gC1q1 domain (Spessotto P. et al.,2003).

- It is also highly expressed along the lymphatic vessels regulating both their structure and function (Danussi C. et al., 2008). In fact, EMILIN1 deficiency results in hyperplasia and enlargement of the superficial and visceral lymphatic vessels, which often display an irregular pattern.

- EMILIN1 deficiency also leads to a significant reduction of the anchoring filaments, and this correlates with the functional defects observed, such as mild lymphedema, an enhanced lymph leakage and a significant decrease of lymph drainage. EMILIN1-deficient mice also develop larger lymphangiomas if compared to wild type mice (Danussi C. et al., 2008). Moreover, EMILIN1 deficiency causes skin and lymphatic vessel hyperplasia and structural anomalies in lymphatic vasculature. Furthermore, an EMILIN1-negative microenvironment promotes tumor cell proliferation as well as the dissemination of cancer cells to the lymph nodes (Danussi C. et al., 2012).

3.6.2 EMILIN2.

EMILIN2 was cloned following a two-yeast hybrid screening using the globular gC1q domain as a bait (Doliana R. et al., 2001). This protein is characterized by a proline-rich (41 %) segment of 56 residues between the coiled-coil region and the collagenous stalk. Differently from EMILIN1, EMILIN2 displays a low expression in adult aorta, small intestine and appendix, whereas the highest levels of the protein can be detected in fetal heart and adult lung mice.
In mouse embryos, EMILIN2 mRNA expression is more restricted compared with that of EMILIN1; early expression includes somites, neural tube and mesenchyme of branchial arches, limb buds, intervertebral disks and perineural tissue. Weak staining is also found in mesenchymal cells of most organs, including lung, liver, intestine and bladder at the beginning of organogenesis. The strongest EMILIN2 expression was detected in the heart, starting at E8.5 and reaching the highest levels at E11.5. Labelling is restricted to the myocardium, while the endocardium is negative. Unlike other members of the family, staining for EMILIN2 was also detected in the central nervous system. In the adult tissues, EMILIN2 mRNA expression is mostly evident in the spleen and the uterus whereas it is weak in kidney and gut (Braghetta P. et al., 2004). Moreover, EMILIN2 was found to be one of the major basilar membrane components in the cochlea (Amma L.L. et al., 2003). At the functional level, EMILIN2 was demonstrated to significantly impair tumor growth inducing tumor cell apoptotic death. EMILIN2 adopts a totally different mechanism from other ECM proteins that promote cell death; in fact, it bears the unique property to directly interact with and activate death receptors, in particular DR4. The activation of the extrinsic apoptotic pathway leads to a dramatic decrease of tumor cell viability and to anti-tumorigenic properties as demonstrated by *in vitro* and *in vivo* studies (Mongiat M. et al., 2007). Moreover, we have recently demonstrated that EMILIN2 exerts an additional anti-proliferative function in the tumor microenvironment. In fact, we have shown that EMILIN2 targets directly breast cancer cells impairing their growth and motility by negatively modulating Wnt signaling activation (Marastoni S. et al., 2014). Interestingly and unexpectedly, EMILIN-2 also stimulates the development of new vessels (Mongiat M. et al., 2010; Broniz A. et al., 2012). The molecular mechanisms by which EMILIN2 could affect ECs behavior and activate angiogenesis were until now unknown, but they have been recently highlighted by our research group and submitted for a publication. Briefly, we found that EMILIN2 produced by fibroblasts induces the activation of EGFR at the EC surface following both a direct binding to the receptor and its ligand EGF. This leads to the activation of the Jak2/STAT3 pathway, IL8 production and a consequent increase of EC proliferation and migration.

In addition, this mechanism is elicited also fibroblasts, thus EMILIN-2 induces the activation both through autocrine and paracrine mechanisms (Fig. 7). The molecular activations prompted by EMILIN-2 were further assessed in various *ex vivo* and *in vivo* experimental settings. In particular, employing a syngenic melanoma cell line in wild-type and *Emilin-2* knock-out mice, we demonstrated that EMILIN-2 deficiency compromised the intratumoral vascularisation and this was associated with a strong reduction of the tumor growth. Interestingly, we also found that in tumors from wild type mice the vessels are more numerous compared to those grown in Emilin-$2^{-/-}$ mice, they display an intact basal lamina and are also better perfused and more efficient in transporting blood and, hence, drugs.

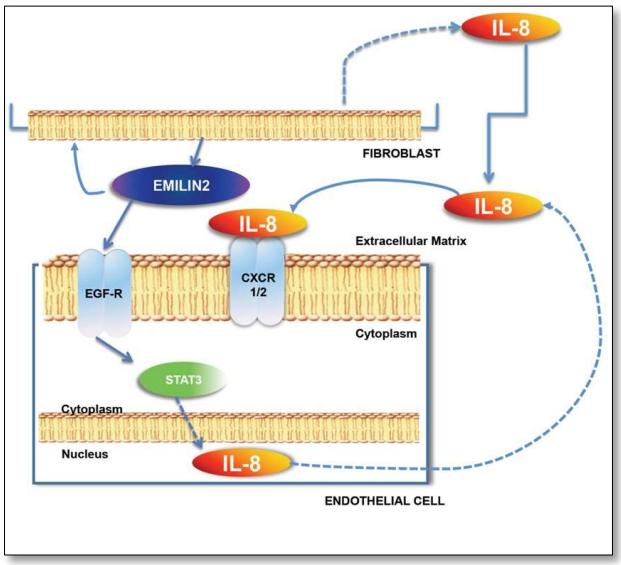

Fig. 7: EMILIN2 activates IL-8 production in ECs and fibroblasts. Schematic representation of the effects of fibroblast- derived EMILIN2 on ECs. EMILIN2 binds to the EGFR thus inducing IL 8 production. As a consequence IL8 activates ECs affecting both their proliferation rate and their motility. Moreover, EMILIN2 induces IL8 expression also in **f**ibroblasts thus acting both in a paracrine and autocrine fashion.

3.6.3 MULTIMERIN1.

MULTIMERIN1 (MMRN1) is a soluble S–S linked homopolymer stored in platelets, megakaryocytes and ECs (Hayward C.P., 1997; Adam F. et al., 2005). It supports the adhesion of platelets, neutrophils, and ECs via integrin αvβ3 and αIIbβ3 (Adam F. et al., 2005). MMRN1 binds to collagen and it is able to enhance von Willebrand factor-dependent platelet adhesion to collagen, thus supporting thrombus formation. MMRN1 has a high affinity for factor V (Jeimi S.B. et al., 2008) and this facilitates the co-storage in platelet α-granules. During platelet activation, MMRN1 is released from platelets, it regulates thrombin production, thus halting thrombus formation. MMRN1 prompts cell adhesion through the RGD sequence present at the N-terminus of the molecule; on the contrary no other domain or motif within the molecule has been held responsible for the other functions exerted by the molecule (Adam F. et al., 2005).

3.6.4 MULTIMERIN2.

MULTIMERIN2 (MMRN2) also known as EndoGlyx-1, was identified during a screening for new antigenic markers of the vascular endothelium, using the monoclonal antibody H572 raised against the human umbilical vein EC (Sanz-Moncasi MP. et al., 1994) (Fig. 8). Unlike other members of the family, MMRN2 is characterized by a short cluster of charged amino acids (10 out of 27 residues) located between the coiled-coil region and the C1q-like domain.

The basic amino acids are arranged in a sequence similar to that of the consensus motifs responsible for the ionic interactions with glucosaminoglycans, such as heparin and heparan sulfate (Hileman RE. et al., 1998) and are also found in heparin binding proteins like the von Willebrand factor (Sobel M. et al., 1992). In an extensive immunohistochemical survey of normal human fetal and adult tissues as well as human cancer tissues, MMRN2 was found to be exclusively expressed at the blood vessel endothelium level. Notably, these include capillaries, veins, arterioles, and muscular arteries. Interestingly, no immunoreactivity was observed in the sinusoidal endothelial cells of the spleen and liver. In neoplastic tissues, MMRN2 was consistently found to be deposited along tumor capillaries and, in certain tumors, in the "hot spots" of neoangiogenesis (Sanz-Moncasi MP. et al., 1994). The staining pattern revealed a uniform cell surface and cytoplasmic distribution of the antigen and, in some cases, an accentuated immunoreactivity at the abluminal side of the EC layer.

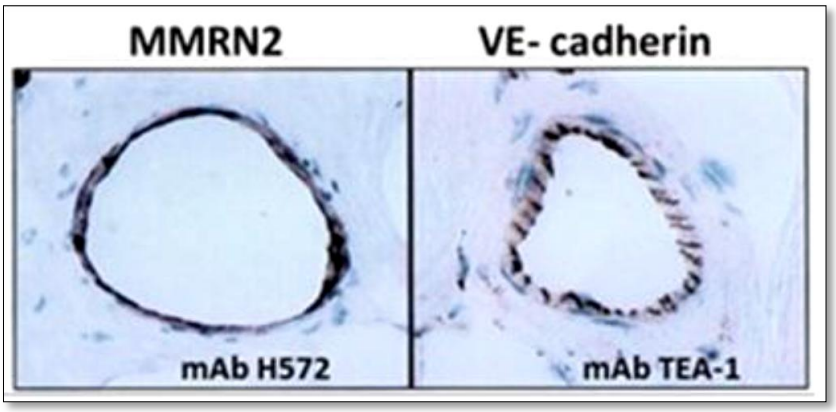

Fig. 8: Immunohistochemical staining of MMRN2 on human blood vessels. Sections of normal breast tissue stained with the H572 mAb detecting MMRN2 or with TEA-1 mAb detecting VE-Cadherin (Christian S. et al., 2001).

Quite recently, we have demonstrated that once over-expressed, MMRN2 halts the development of new blood vessels and induces a strong inhibition of tumor growth (Lorenzon E. et al., 2012). The molecule plays an important role in the regulation of EC behavior negatively affecting EC motility and inducing a significant impairment of angiogenesis. In our study, we identified the molecular mechanism responsible of these effects which rely, at least in part, on the binding of VEGF-A to MMRN2. A more in-depth analysis on the anti-angiogenic effect of MMRN2, the identification of the active region of the molecule responsible of this effect as well as the investigation of the putative role of MMRN2 in the regulation of EC homeostasis have been the subject of my PhD program and will be further detailed in this thesis.

4. AIMS OF STUDY

The ECM molecule MULTIMERIN2 (MMRN2), secreted by ECs and deposited along the vasculature in tight juxtaposition with these cells, is a strong inhibitor of angiogenesis. In our laboratory we have previously demonstrated that the over-expression of this molecule affects ECs' behavior inducing a strong reduction of their motility. This effect is due, at least in part, to a direct binding of MMRN2 to VEGF-A_{165}, which in turn results in a significant inhibition of the VEGF-A/VEGFR2 signaling axis. Moreover, we have found that the angiostatic effects induced by the over-expression of MMRN2 lead to an impressive impairment of tumor growth and a strong decrease of the density of the tumor-associated vessels. Starting from these promising evidences we thought to better elucidate the role of MMRN2 in this context and in particular to:

1) Identify the region of MMRN2 involved in the interaction to VEGF-A_{165} and responsible for its anti-angiogenic effect. Moreover we intended to investigate if this interaction is mediated by oligosaccharides or by the protein core of the molecule. In addition, we were interested to verify if MMRN2 or its putative active fragment bound to other VEGF-A isoforms and/or other VEGF family members involved in angiogenesis.

2) Assess if MMRN2, given its strategic deposition along the vessels could be an important regulator of vascular homeostasis, playing a part in vessels' stability and maturation and vascular permeability.

5. MATERIALS AND METHODS

5.1 Cell cultures.

Human Umbilical Vein Endothelial Cells (HUVEC) were isolated from the human umbilical cord vein as previously described (Jaffe EA et al., 1973). Cells were cultured in M199 medium (GIBCO, Invitrogen, Milan, Italy) supplemented with 20% fetal bovine serum (FBS) (GIBCO, Invitrogen, Milan, Italy), 1% Penicillin-Streptomycin (Sigma-Aldrich, Milan, Italy), 50 mg/ml heparin (Sigma-Aldrich, Milan, Italy) and bovine brain extract (0,5%). Embryonic kidney 293-EBNA (Epstein-Barr Nuclear Antigen) cells were a gift from Rupert Timpl (Max Planck, Munich, Germany) and were cultured in Dulbecco's modified Eagle medium (DMEM) (Sigma-Aldrich, Milan, Italy) containing 10% FBS, 1% Penicillin-Streptomycin and 250 µg/ml of G418 (Sigma-Aldrich, Milan, Italy); 0.5 µg/ml of puromycin (Sigma-Aldrich, Milan, Italy) were added after transfection. The human fibrosarcoma (HT1080) cell line was obtained from American Type Culture Collection (ATCC, Manassas, VA) and cultured in DMEM containing 10% FBS, 1% Penicillin-Streptomycin and 600 µg/ml of G418 after transfection. Normal human dermal fibroblast (NHDF) cells were obtained from LONZA (Basel, Switzerland) and maintained in DMEN supplemented with 10% FBS and 1% Penicillin-Streptomycin. All cells were maintained at 37°C in a humidified 5% CO_2 atmosphere.

5.2 Antibodies and other reagents.

The anti-histidine antibody was from Abgent (San Diego, CA, USA), the Ni-NTA agarose was from QIAGEN (Milan, Italy). The anti-MMRN2 polyclonal antibody was obtained upon immunization of a rabbit with 150 µg of a recombinant MMRN2 fragment corresponding to the N-terminal gC1q domain. The antibody was affinity purified from the rabbit serum by means of the CNBr-activated Sepharose 4B resin (Amersham, GE-Healthcare, Milan, Italy). The secondary horse radish peroxidase (hrp)-conjugated antibodies were from Amersham (GE-Healthcare, Milan, Italy). The secondary antibodies conjugated with Alexa Fluor 488, 568 and TO-PRO-3 were from Invitrogen (Milan, Italy). Recombinant human VEGF-$A_{165,}$ VEGF-$A_{145,}$ VEGF-A_{189} proteins were from R&D systems, Inc (MN,USA) and $VEGF_{121}$ from Peprotech (London, UK). The basic FGF, VEGF-B_{167} was from Peprotech (Rocky Hill, NJ). The anti-SMA was from Abcam (Cambridge, UK). The anti-CD31 antibody and Matrigel were from BD Biosciences. The anti-VEGFR2 and anti phospho-VEGFR2 (Tyr1175) and (Tyr1214), the anti-p38 and anti-phospho-p38, and the anti-β-actin and the anti-VE-cadherin antibodies were from Cell Signaling Technology Inc. (Danvers, MA, USA). The anti-ZO-1 and the anti-occludin antibodies were from Invitrogen (Life Technologies Italia, Monza, Italy) The anti-VEGF-A antibody was from Sigma-Aldrich (Milan, Italy). Anti-VEGF-B, anti-VEGF-C, anti-VEGF-D and anti-PlGF were from Santa Cruz Biotechology Inc. (California, USA). The *in situ* Cell Death Detection Fluorescein Kit was purchased from Roche Diagnostics S.p.a. (Milan, Italy). Cytodex 3 microcarriers were from GE Healthcare Life Sciences (Milan, Italy). Drabkin reagent kit and Tunicamycin and FITC-dextran (70kDa) were purchased from Sigma-Aldrich (Milan, Italy); AngioSense® 750EX fluorescent imaging agent was from PerkinElmer (Waltham, Massachusetts). HBVP (Human Brain Vascular Pericytes) cell lines was obtained from SciencCell (Carlsband, CA, USA)

5.3 DNA constucts.

The following MMRN2 deletion mutants were created: Δ1 (aa residues 24 to 474), Δ2 (aa residues 137 to 336), Δ3 (aa residues 348 to 683) and Δ4 (aa residues 674 to 949). The fragments were amplified from the full length molecule and cloned into the pCEP-Pu vector containing the BM40 signal peptide sequence using the following oligonucleotides: Δ1: 5'-CTAGCTAGCCCATCATCACCATCACCATGCTTCCAGTACTAGCCTC-3' containing the NheI site and His sequence; 5'-ATAGTTTAGCGGCCGCTCAGAGGTTGAGCTCCAGGAG-3' containing the NotI site; Δ2: 5'-CTAGCTAGCCCCATCATCACCATCACCATCCAATCCCTGAGCCTGCA-3' containing the NheI site and His sequence; 5'-ATAGTTTAGCGGCCGCTCATTTGGTGTCCACATCGGC-3' containing the NotI site; Δ3: 5'-GCAACAGCTGTCCATCATCACCATCACCATGGGACCAATGGCAGTCTGGTG-3' containing the pshAI site and the His sequence; 5'-CGGGATCCGTCGTGGCTGGGCTCCAG-3' containing the BamHI site; Δ4: 5'-GCTAGCCCATCATCACCATCACCATCCGGCAGAGCACCTGGAG-3' containing the NheI site and His sequence; 5'-ATAGTTTAGCGGCCGCTCATCAGGTCTTAAACATCAGG-3' containing the NotI site. In addition, the MMRN2 or Δ2 cDNA were sub-cloned into pcDNA3.1/Myc-His vector by *Hind* III and *Bam* HI restriction. RNA was extracted from tumor frozen sections with the Trizol reagent (Invitrogen, Milan, Italy)., and reverse transcription performed using AMV-RT and exanucleotides (Promega, Milan, Italy). Real-time PCRs were carried out using the iQ™ SYBR® Green Supermix (Bio-Rad, Hercules, CA, USA) using the following oligonucleotides: GAPDH 5′-GAGAGACCCTCACTGCTG-3′, 5′-GATGGTACATGACAAGGTGC-3′; HIF- 1α 5′-CAGAGCAGGAAAAGGAGTCA-3′, 5′-AGTAGCTGCATGATCGTCTG-3′; The primer efficiency was ~100%, thus the comparative Ct method (2−ΔΔCt) was applied for the analyses.

5.4 Cell transfection, expression and purification of recombinant proteins.

293-EBNA cells were transfected by electroporation with the different pCEP-Pu constructs and selected in the presence of 0,5 µg/ml of puromycin and 250 µg/ml of G418. Positive clones were isolated and the expression analyzed by Western blotting. Confluent 293-EBNA cells were then incubated in serum-free medium for 48 hours, the media were collected and equilibrated with a buffer containing 50 mM NaH_2PO_4, 150 mM NaCl, 10 mM imidazole. The proteins were purified by means of the Ni-NTA resin and eluted with the elution buffer (50 mM NaH_2PO_4, 300 mM NaCl, 250 mM imidazole). The different fractions were analyzed by SDS-PAGE followed by Coomassie blue staining. Protein fractions were then dialyzed against PBS and concentrated using polyethylene glycol (PEG). In addition, HT1080 cells were stably transfected by electroporation with the pcDNA constructs and selected in the presence of 600 µg/ml of G418.

5.5 Scratch test and cell migration assay.

For the scratch test HUVEC cells were seeded in a 24-multiwell dish and allowed to grow until they reached confluency. Cells were then starved overnight and the day after a scratch wound across each well was made using a sterile pipet tip. Cells were washed to remove any loosely held cells and then incubated with medium containing 0,5 % serum in the presence of 5 µg/ml of purified MMRN2 or the equimolar concentrations (35nM) of Δ1, Δ2, Δ3 and Δ4 purified fragments, or type I collagen as a control. The open gap was then inspected over time with the microscope. Time course analysis was carried out by means of the LEICA AF6000 Imaging System (LEICA, Wetzlar, Germany).
For the motility assay the transwell membranes carrying 8 µm pores were coated on the upper side with 5 µg/ml of MMRN2 or the equimolar concentrations (35nM) of Δ1 or Δ2 or Δ3 or Δ4 fragments in the presence of 0,1M bicarbonate buffer pH 9,6 at 4°C overnight. Type I collagen was used as control. The next day the membranes were saturated with 1% BSA in PBS for 1 hour at room temperature. $1x10^5$ HUVEC cells were placed on the top layer of the permeable membrane in serum free M199 medium containing 0,1% BSA. In the bottom chamber VEGF-A was added to the medium as migratory stimulus at the concentration of 25 ng/ml. After 6 hours of migration cells were stained with Crystal violet for 30 minutes and counted.

5.6 Cell viability and proliferation assay.

HUVEC cells were incubated with 35 nM of MMRN2 or PBS for 24, 48 and 72 hours; in alternative the cells were challenged with MMRN2, collagen type I and the various deletion mutants for 48 hours and cell viability was analyzed. The MTT (3-(4,5-Dimethylthiazol- 2-yl)-2,5-diphenyltetrazolium bromide, a tetrazole) reagent was added to the cells at a final concentration of 0,3 mg/ml and incubated for 4 hours at 37°C in complete medium. The medium was discarded and the crystals solubilized with dimethyl sulfoxide (DMSO). The reduced form of the colorimetric substrate was then quantified at the spectrophotometer at 560 nm. Cell proliferation was assessed by culturing the mock and Δ2-transfected HT1080 cells in 96-well plates for 24, 48, 72 and 96 hours. Cells were stained with the Trypan blue solution (Sigma-Aldrich, Milan, Italy) and counted using a hematocytometer.

5.7 TUNEL assay.

The apoptotic rate was evaluated using the "in situ cell death detection kit, fluorescein" (Roche Diagnostics S.p.a, Milan, Italy) upon treatment of HUVEC cells with 5µg/mL recombinant MMRN2 or with the equimolar concentrations (35nM) of Δ1, Δ2, Δ3 and Δ4 purified fragments for 48 hours, and the assay performed according to the manufacturer's instructions. Lipopolysaccharides from Salmonella enteric Serotype enteritidis (LPS, Sigma-Aldrich, Milan, Italy) at the concentration of 100 ng/ml was used to induce HUVEC cell apoptosis. Briefly, the cells were fixed in 4% PFA for 20 minutes at room temperature, permeabilized for 2 minutes in freshly prepared permeabilization solution (sodium citrate 0,1%, Triton X-100 0,1%) at 4°C and incubated with the properly diluted enzyme solution for 1 hour at 37°C in humidified conditions.

The cells were mounted in Fluoroshield™ with DAPI (Sigma-Aldrich, Milan, Italy) and positive cells counted using a fluorescence microscope equipped with a 63X objective. The same protocol was used to score the apoptotic rate in HT1080 cells stably expressing the Δ2 fragment of MMRN2.

5.8 Matrigel tube formation assay.

The growth factor reduced Matrigel TM Matrix (BD Biosciences) was thawed at 4°C overnight; 40 µl were quickly added to each well of a 96-multiwell dish using cold pipettes and was allowed to solidify for 30 min at 37°C. Once solid, $1x10^4$ HUVEC cells were resuspended in medium containing 0,5% serum and 5 µg/ml of purified MMRN2 or the equimolar concentrations (35nM) of Δ1, Δ2, Δ3 or Δ4 purified fragments, or type I collagen as a control and then seeded in each well. Time-course analyses was carried out for 12 hours by means of LEICA AF6000 Imaging System. Tube formation analysis was assessed with the Wimasis software

5.9 3D *in vitro* angiogenesis assay.

The 3D in vitro spheroid based angiogenesis tests were performed as previously described (Nakatsu MN. et al., 2007). Briefly, $4x10^2$ HUVEC cells per cytodex microcarrier were employed. ECs were incubated with the beads for 4 hours at 37°C, shaking every 20 minutes. After the incubation time, the coated beads were transferred into a flask containing complete medium and were incubated overnight at 37°C. The next day the coated beads were embedded into a fibrin gel with or without 35nM of MMRN2 or the Δ1, Δ2, Δ3 and Δ4 purified fragments. To provide the required soluble factors to promote EC sprouting, NHDF cells were layered on top of the gel after resuspension in medium containing the purified fragments, in combination or not with VEGF-A (50 ng/ml). After 7 days spheroids were fixed with 4% (w/v) paraformaldehyde for 15 minutes at room temperature and pictures were captured and analyzed by Image J software.

5.10 ELISA test.

For the analysis of the binding of MMRN2 or Δ1, Δ2, Δ3 and Δ4 fragments with VEGF-A, 0.5 µg of the recombinant MMRN2 or the deletion mutants were used to coat the plates and BSA was used as a control. The wells were blocked with 2% BSA in PBS for 1 hour at room temperature and incubated with soluble VEGF-A (100 ng/well) in 0,2% BSA in PBS for 1 hour at 37°C. In other sets of experiments, the MMRN2-coated wells were incubated with soluble VEGF-B, VEGF-C, VEGF-D or PlGF. Binding was verified using the specific anti-cytokine antibodies; the ABTS substrate was added and absorbance at 405 nm detected with a spectrophotometer (TECAN, Milan, Italy).

5.11 Surface plasmon resonance tests.

The affinity measurements were performed using a Biacore X100 biosensor (GE Healthcare) on a carboxymethyldextran-coated sensor chip (CM5) as previously described (Lorenzon E. et al., 2012). The purified MMRN2 (20 ng/ µl) or the Δ2 fragment (80 ng/µl) in Na acetate pH=4 were immobilized using amine coupling to a density of 3150 and 1770 resonance units (RU), respectively. VEGF-A_{165} and VEGF-A_{121}, VEGF-B_{167}, VEGF-C, VEGF-D and PlGF-1 were diluted in HBS-EP buffer (GE Healthcare) at different concentrations and injected over the sensor chip at a flow rate of 30 µL/min, with 60 seconds of analyte contact over the surface. In other sets of experiments when analyzing the interaction with VEGF-A145 and VEGF-A_{189}, a NaCl concentration of 300 mM instead of 150 mM was employed. The kinetic parameters and dissociation constants (kD) were then determined using the BIAevaluation software.

5.12 Deglycosylation and Tunicamicyn treatment.

The cleavage of the MMRN2 carbohydrate chains was performed using the protein deglycosylation kit purchased from New England Biolabs (Beverly, MA) according to manufacturer's instructions. Briefly, 50 µg of purified MMRN2 were incubated with deglycosylation mix under non denaturing or denaturing conditions for 4 hours at 37°C. The deglycosylated protein was used for the analysis of the MMRN2/VEGF-A interaction by ELISA test, as previously described.
For the inhibition of N-linked glycosylation, 293-EBNA cell stably expressing MMRN2 or Δ2 fragment were treated or not with 5 µg/ml of Tunicamycin every 2 hours for 24 hours in serum free medium. The non-glycosylated purified proteins were analyzed by Western blotting and used in the solid phase analysis to evaluate the binding with VEGF-A.

5.13 Preparation of cell lysates and Western blot analysis.

For the phosphorylation studies, HUVEC cells were treated with VEGF-A (15 ng/ml) with or without MMRN2 (5 µg/ml) or the equimolar concentration (35 nM) of the Δ2 purified fragment for different times. The cells were then lysed in cold buffer (1 mM CaCl2, 1 mM MgCl2, 15 mM Tris-HCl pH 7.2, 150 mM NaCl, 1% TrytonX100, 0,1% SDS, 0,1% Na Deoxycholate) containing 25 mM NaF, 1 mM DTT, 1 mM Na3VO4 and the protease inhibitors cocktail (Roche). For the Western blot analyses proteins were resolved in 4-20% Criterion Precast Gels (Bio-Rad Laboratories) and transferred onto Hybond-ECL nitrocellulose membranes (Amersham, GE-Healthcare). Membranes were blocked with 5% BSA in TBS-T (100mM Tris-HCl pH 7.5, 0,9% NaCl, 0,1% Tween 20) and probed with the appropriate antibodies. The blots were finally developed using ECL (Western blotting detection, Amersham Biosciences) and exposed to X-ray films or acquired using the ChemiDoc Touch Imaging System (BIO RAD, Hercules, CA, USA). Alternatively the Odyssey infrared imaging system was used (Li-COR Biosciences, Lincoln, NE, USA).

5.14 Matrigel plug angiogenesis assay.

Ten female BALB/c (Harlan S.r.l, Milan, Italy) mice were subcutaneously injected (0.5 ml/flank) with highly-concentrated (18 mg/ml) Matrigel containing PBS (five left flanks) or 50 ng/ml of b-FGF and VEGF-A (five left flanks) or 50ng/ml of b-FGF and VEGF-A with 35 nM of MMRN2 or Δ2 (10 right flanks). Every other day the growth factors and the recombinant proteins were re-injected into the plugs into a final volume of 100µl. After 10 days, the mice were sacrificed and the Matrigel plugs were excised. The plugs were divided in two parts, one half was fixed with formalin overnight, embedded in paraffin and sectioned onto slides stained with hematoxylin and eosin for histological observation. The remaining plugs were homogenized and the hemoglobin content was evaluated using the Drabkin reagent kit (Sigma-Aldrich, Milan, Italy), as previously described (Kang K. and Lim JS., 2012).

5.15 *In vivo* tumor growth.

Twenty female athymic nude mice (Harlan S.r.l, Milan, Italy) were injected with $1.5x10^6$ of HT1080 cells stably transfected with pcDNA3.1 vector carrying the MMRN2 or Δ2 coding sequence or with the empty vector. The left flanks of each mouse were injected with control cells, while the right flanks with cells expressing MMRN2 or Δ2. Tumor growth was monitored over time and tumor size measured with a caliper. The tumor volumes were calculated with the following formula: $(\Pi x length x width^2)/6$. Tumor vascularity was imaged using AngioSense® 750EX (PerkinElmer). Anesthetized mice were retro-orbital injected with 2 nmol of AngioSense® 750EX in 100 µL of PBS and the fluorescence signal detected after 24 hour by IVIS Lumina instrument (Perkinelmer, Walthman, MA, USA). The mice were sacrificed and the tumors excised for immunofluorescence analysis. All the *in vivo* studies were approved by the Institutional Ethics Committee.

5.16 Immunofluorescence analysis of ECs, tumors sections and whole mount retinas

HUVEC cells were grown on cover glass slides placed in a 24 multi-well plate and treated with VEGF-A (10 ng/ml) and MMRN2 (5 µg/ml) or equimolar concentration (35nM) of Δ2 for 20 min at 37°C and then fixed with 4% (w/v) paraformaldehyde for 15 minutes at room temperature. The cells were permeabilized with a PBS solution containing 1% BSA, 0,2% TRITON X-100 for 5 minutes at room temperature, saturated with blocking buffer (PBS-2% BSA) for 1 hour and incubated overnight at 4°C with the α-VEGFR2 antibody. Next, the actin cytoskeleton and the nuclei were stained for 1 hour at room temperature with phalloidin and TO-PRO3, respectively. Slides were finally mounted in Mowiol containing 2,5% (w/v) of 1,4-diazabicyclo-(2,2,2)-octane (DABCO). The number of cells displaying VEGFR2 staining at the cell surface was evaluated by counting. Alternatively, HUVEC cells were grown on cover glasses, alone or in co-colture with HBVP (Human Brain Vascular Pericytes) at different ratio and incubated with α-human MMRN2 and α-human SMA antibodies.

For immunofluorescence analyses with α-zona occludens (ZO-1), α-occludin (OCLN) and VE-cadherin antibodies, HUVEC cells were transducted with MMRN2 siRNA or control adenoviral vectors and grown on cover glass slides until they reached the confluence. Then, the cells were fixed for 15 min at room temperature in 4% PFA diluted in PBS, washed 3 × 5 min, incubated in 0.1% Triton X-100 (diluted in PBS) for 10 min at room temeprature, washed 3 × 2 min and then incubated in 50 mM Glycine in PBS for 10 min at room temperature. After washing 3 × 5 min, the coverslips were incubated with primary antibody solution (containing 1% BSA in PBS) for 1 hour at room temperature. Samples where then washed 3 × 10 min and the secondary antibodies were incubated in the same manner. Finally, coverslips where washed for 3 × 10 min and mounted using Mowiol containing 2,5% DABCO.

For the immunofluorescence analyses of tumor sections, tumors were included in the Optimal Cutting Temperature compound (OCT) and frozen. For microvessel density analysis, 7 µm thick sections were obtained and stained with anti-mouse CD31.

Images were acquired with a Leica TCS SP2 confocal system (Leica Microsystems Heidelberg, Mannheim, Germany), using the Leica Confocal Software (LCS) and vessel density was assessed by counting.

For the retinal immunostainings, the retinas were isolated as previously described (Pitulescu M. et. al., 2010) from adult wild-type and knock-out C57BL/6 mice. The retinas were fixed in 4% PFA for 2 hours at 4°C and saturated overnight at 4°C with the blocking buffer (PBS-1% BSA-0,3% TRITON X-100). The next day the specimens were incubated overnight at 4°C with the anti-MMRN2 antibody and with mouse anti-SMA. After incubation, the retinas were washed with PBS 5 times for 20 minutes, incubated with the specific secondary antibody for 2 hours at room temperature and washed 4 times for 20 minutes. Finally, the samples were mounted using Mowiol with 2,5% DABCO and the images were acquired with a confocal system (Leica Microsystems).

5.17 Adhesion assay.

For the adhesion assays 96 well-plates were coated with 10 µg/ml of MMRN2 or collagen type I at 4°C. After an overnight incubation with the proteins, the solution was removed and the plate air-dried at room temperature in a tissue-culture hood. Next, previously starved HBVP cells were resuspended in a medium containing 0.1% BSA and added to each well at a number of $2x10^5$ cells/ml. The plate was placed for 1 hour in the cell incubator at 37°C, next the cells were washed and stained with Crystal Violet. The extent of adhesion was assessed by measuring the Absorbance at 560 nm.

To quantitatively monitor cell adhesion over time we exploited the xCELLigence Real Time dual plate Cell Analyzer (Roche). The 96 well E-Plates were pre-coated with 10 µg/ml of MMRN2 or collagen type I at 4°C overnight and HBVP cells were then seeded at a number of $5.0x10^4$ cells/well. Cell adhesion, measured as changes in impedance and recorded in arbitrary cell index (CI) units, was monitored every 5 minutes for 130 minutes.

5.18 Permeability assay.

For this test, HUVEC cells ($2x10^4$) were seeded on collagen type I-coated Transwell filters (1µm mm pore size, BD Biosciences) in 24-well dishes and cultured with 100 ml of complete Medium in the upper chamber and 600 ml of growth medium in the lower chamber. The cells were grown for five days without medium changes until they had reached confluence. Then, using sterile tweezers, each insert was picked up and the media gently removed. The inserts were washed with PBS and transferred to other fresh plates. Finally, 200 µl of growth medium containing FITC-Dextran 70 kD (1:100) were added to the upper chambers and 600µl of growth medium to the lower chamber. FITC-Dextran concentration was measured from the lower chambers by means of TECAN Infinity 200 PRO instrument detecting the fluorescence at 535 nm.

5.19 *In vivo* permeability: FITC-dextran perfusion assay.

To analyze VEGF-induced acute permeability responses, 100µl of PBS or VEGF-A_{165} at a final concentration of 50 ng/ml were injected intradermally in the ear of wild-type or MMRN2 knock-out C57BL/6 mice, followed by retrorbital injection of 100µl of FITC-dextran (50 ng/ml in PBS). After 30 minutes, mice were sacrificed, ear tissues were excised and fixed with 4% PFA. FITC-Dextran leakage from the vessels was assessed by immunofluoresce analyses from the fluorescent stereo-microscope's images.

5.20 Statistical analyses.

Statistical analyses were performed using the Sigma Plot software. Student t-test for unpaired data was used to assess the probability of significant differences between two groups; for more than two groups, the ANOVA 1-way analysis of variance was used, according to the Bonferroni method. Results with $p \leq 0.05$ were considered significant.

6. RESULTS

6.1 Production and expression of four MMRN2 deletion mutants.

In order to identify the active region of MMRN2 involved in the interaction with VEGF-A_{165} and in its anti-angiogenic effect, we firstly generated 4 deletion mutants. In particular we created the Δ1 (aa residues 24 to 474), Δ2 (aa residues 137 to 336), Δ3 (aa residues 348 to 683) and Δ4 (aa residues 674 to 949) deletion fragments. All these fragments were amplified from the full length molecule, cloned into the pCEP-Pu vector and expressed in 293-EBNA cells (Fig. 1A). Then, the expression of purified His-tagged deletion mutants was evaluated by Western blot analysis (Fig. 1B).

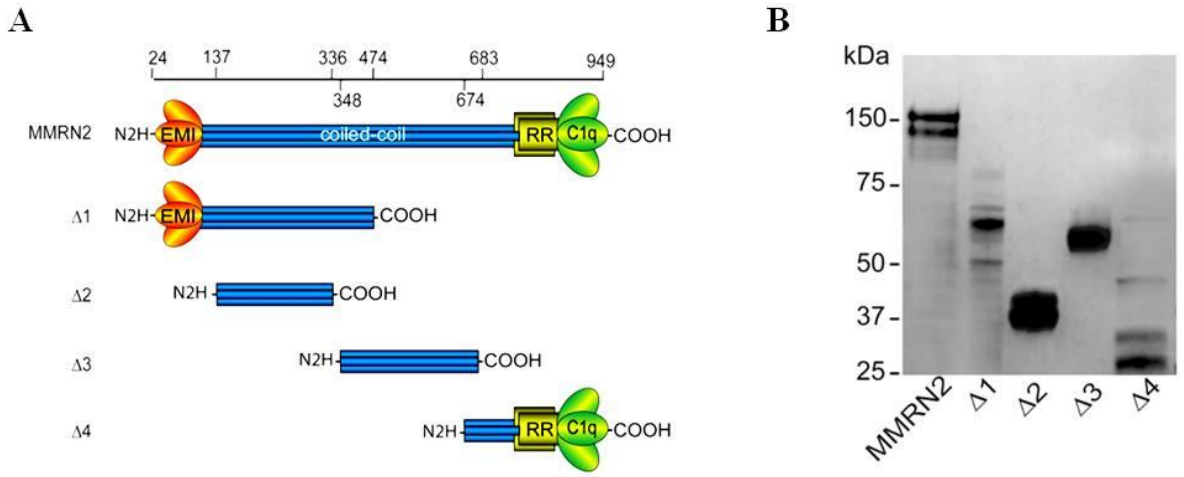

Fig. 1: Schematic representation and analysis of the MMRN2 deletion mutants. (A) Schematic representation of the various MMRN2 deletion mutants (Δ1 to Δ4). The position number of the amino acid residues of the deletions is reported on top and excludes the first 24 residues of the signal peptide. The EMI domain (EMI), the coiled-coil region, the Arginine-rich domain (RR) and the gC1q domain (C1q) are indicated. **(B)** Western blot analysis of the His-tagged MMRN2 molecule and the various recombinant deletion mutants (Δ1 to Δ4) purified by means of the Ni-NTA resin. An anti-His antibody was used for the analysis.

6.2 Analysis of the biological effects of the MMRN2 deletion mutants on ECs.

Firstly, we verified if MMRN2 could affect the proliferation of HUVEC cells over time. For this purpose, HUVEC cells were incubated with 5μ/ml of MMRN2 for 24, 48 and 72 hours and we did not find significant changes in ECs' viability (Fig. 2A). Thus, we decided to repeat the experiment only at 48 hours treating HUVEC cells with the equimolar concentration (35 nM) of MMRN2 and the various deletion mutants. In accordance with what found with the whole molecule, also the recombinant fragments did not affect the proliferation of ECs (Fig. 2B). Subsequently, we also assessed whether the deletion mutants, as the entire molecule, had no effect on EC apoptotic rate. To this end, the HUVEC cells were treated for 48 hours with 5 μg/ml of MMRN2 or with equimolar concentrations (35 nM) of the purified fragments or type I collagen used as a control. Following the treatment we evaluated the percent of apoptotic ECs by means of TUNEL assays.

As shown in Fig. 2C, similarly to what obtained with the entire molecule, the MMRN2 deletion mutants did not alter the percentage of ECs undergoing apoptosis.

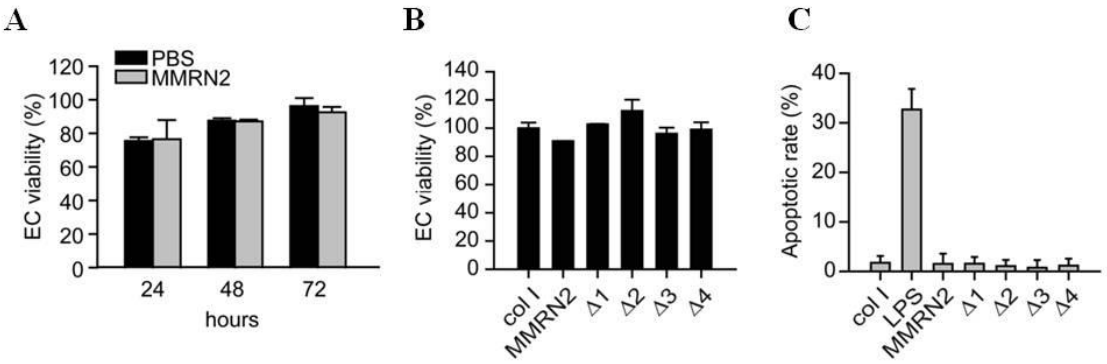

Fig. 2: **The MMRN2 deletion mutants do not alter proliferation or apoptotic rates of ECs. (A)** Graph representing the % of cell viability of HUVEC cells challenged with 35 nM of MMRN2 or vehicle (PBS), following 24, 48 and 72 hours of incubation, as assessed by MTT assays. **(B)** Graph representing the % of cell viability of HUVEC cells challenged with equimolar concentrations (35 nM) of type I collagen (col I), MMRN2 or the deletion mutants (Δ1 to Δ4) performed after 48 hours of incubation. **(C)** Graph representing the % of apoptotic HUVEC cells challenged with equimolar concentrations of type I collagen (col I), MMRN2 or the deletion mutants (Δ1 to Δ4) as obtained by TUNEL assays performed after 48 hours of incubation; 100 ng/ml of LPS were used to induce apoptosis. P values were obtained with the ANOVA one way analysis of variance and graphs represent the mean ± SD obtained from at least three experiments.

As carried out for the whole molecule, the purified deletion mutants were tested for their ability to inhibit EC migration. First we performed a scratch assay. To this end, HUVEC cells were seeded on 24-multiwell plates, allowed to grow to confluency and then, a scratch wound across each well was made using a sterile pipet tip. Next, the cells were treated with 5 µg/ml of purified MMRN2 or with the equimolar concentrations (35 nM) of the four purified fragments and the EC movement across the area was monitored by time lapse analysis. After 6 hours, we found that, similarly to the effect exerted by the entire molecule, the Δ1 and Δ2 mutants were able to significantly inhibit the migration of HUVEC cells. On the contrary, as shown in Fig. 3A and Fig. 3B, Δ3 and Δ4 deletion mutants did not affect cell motility. These results were also corroborated by migration assays performed on transwells. In this case, 5 µg/ml of MMRN2 or equimolar concentrations (35 nM) of the Δ1, Δ2, Δ3, Δ4 purified fragments were coated on the upper side of transwell membranes. HUVEC cells were then placed on the top of the inserts' membrane and let migrate towards a VEGF-A_{165} stimulus at the concentration of 25 ng/ml. Also in this case, we found that only Δ1 and Δ2 deletion mutants were able to halt the motility of HUVEC cells (Fig. 3C).

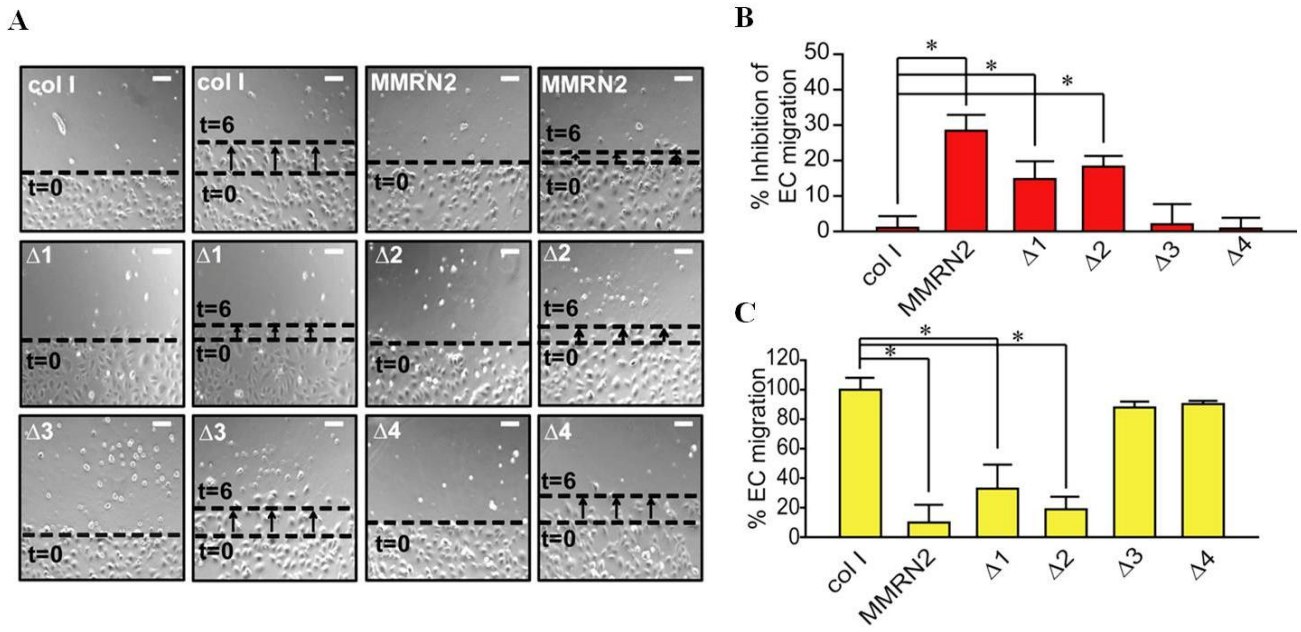

Fig. 3: MMRN2 and its active mutants impair EC motility. (A) Representative images of the scratch test assay. HUVEC cells were treated with equimolar concentrations (35 nM) of MMRN2 and the various recombinant deletion mutants (Δ1 to Δ4); type I collagen was used as control and the front of cell migration at time zero (t=0) and after 6 hours (t=6) are highlighted; scale bar = 145 μm. **(B)** Graph representing the analysis of the scratch test expressed as the % of inhibition of EC' migration respect to the collagen control; (*P ≤0.026). **(C)** Graph representing the migration on transwells of HUVEC cells challenged with equimolar concentrations (35 nM) of type I collagen (col I), MMRN2 or the deletion mutants (Δ1 to Δ4); (*P ≤ 0.001). P values were obtained with the ANOVA one way analysis of variance and graphs represent the mean ± SD obtained from at least three experiments.

6.3 Effect of the MMRN2 deletion mutants on ECs in 2D and 3D contexts.

To further assess the influence of MMRN2 or its deletion mutants in affecting EC behavior, we carried out a tube formation assay on Matrigel. Indeed, the differentiation and reorganization of ECs to form tubules is one of key steps occurring during the angiogenic process. To verify the role of MMRN2 and its deletion mutants in this context, HUVEC cells were resuspended in a medium containing 5 μg/ml of MMRN2 or the equimolar concentrations (35 nM) of the purified fragments or type I collagen and then seeded on a pre-solidified matrigel matrix. The experiment was monitored over time by time-lapse microscopy and the analyses performed on the images captured at 12 hours of incubation. As shown in Fig. 4A to 4G, either the entire molecule or the Δ1 and Δ2 deletion mutants strongly impaired the ability of ECs to form tubules on Matrigel. Conversely, when treated with type I collagen or Δ3 and Δ4 the ECs were able to form a complete vessel network.

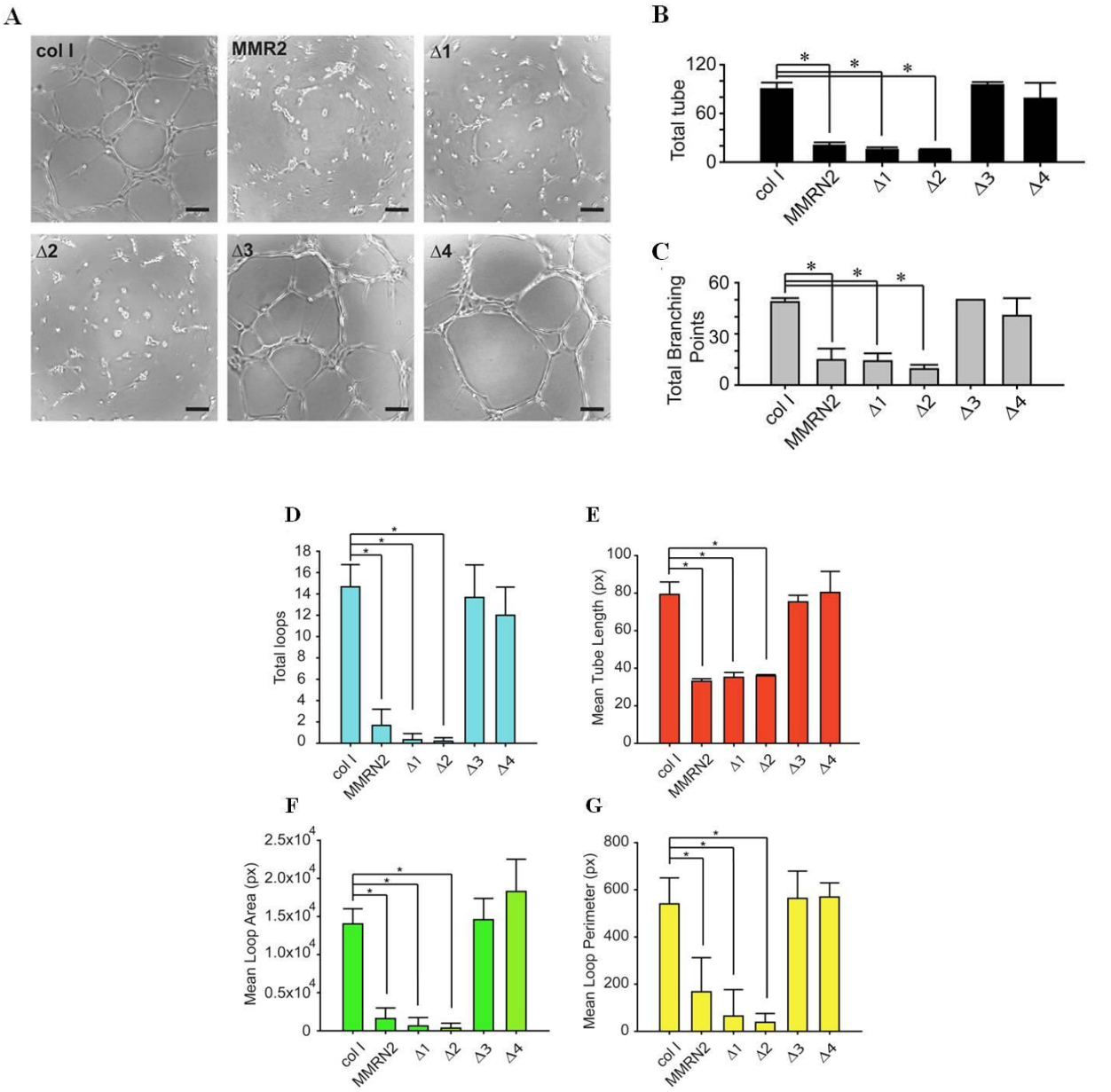

Fig. 4: MMRN2 and its active mutants impair tubuligenesis on Matrigel. (A) Representative images of a matrigel tubulogenesis assay upon treatment of HUVEC cells with equimolar concentrations (35 nM) of the various recombinant molecules under analysis. Type I collagen was used as control; scale bar = 100 μm. **(B)** and **(C)** Graphs representing the evaluation of the number of tubes and total branching points as obtained from the experiment in A by means of with the Wimasis tube analysis software; (*P < 0.001). **(D), (E), (F)** and **(G),** Graphs representing the analysis of respectively, the total loops (*P < 0.001), the mean tube length (*P < 0.012), the mean loop area (*P < 0.001) and the mean loop perimeter (*P ≤ 0.001) obtained from the experiment reported in A and assessed by the Wimasis tube analysis software. P values were obtained with the ANOVA one way analysis of variance and graphs represent the mean ± SD obtained from at least three experiments.

Subsequently, to better resemble the physiological condition, the development of novel vessels was assessed in a 3D context following the treatment with MMRN2 or the various deletion mutants. To this end, we performed a spheroid-based 3D angiogenesis test, in which EC spheroids embedded in a fibrin gel and overlaid with Normal Human Dermal Fibrobalst (NHDF) were challenged with the recombinant molecules under analysis in combination or not with VEGF-A_{165} (50 ng/ml). As shown in Fig. 5A MMRN2 and the Δ1 and Δ2 mutants strongly hampered the sprouting of ECs. In particular, both the number and the length of the sprouts were significantly decreased when compared to those obtained with the control or following the treatment with Δ3 and Δ4. This effect become even more stronger in presence of VEGF-A_{165} at the concentration of 50ng/ml (Fig. 5B and 5C).

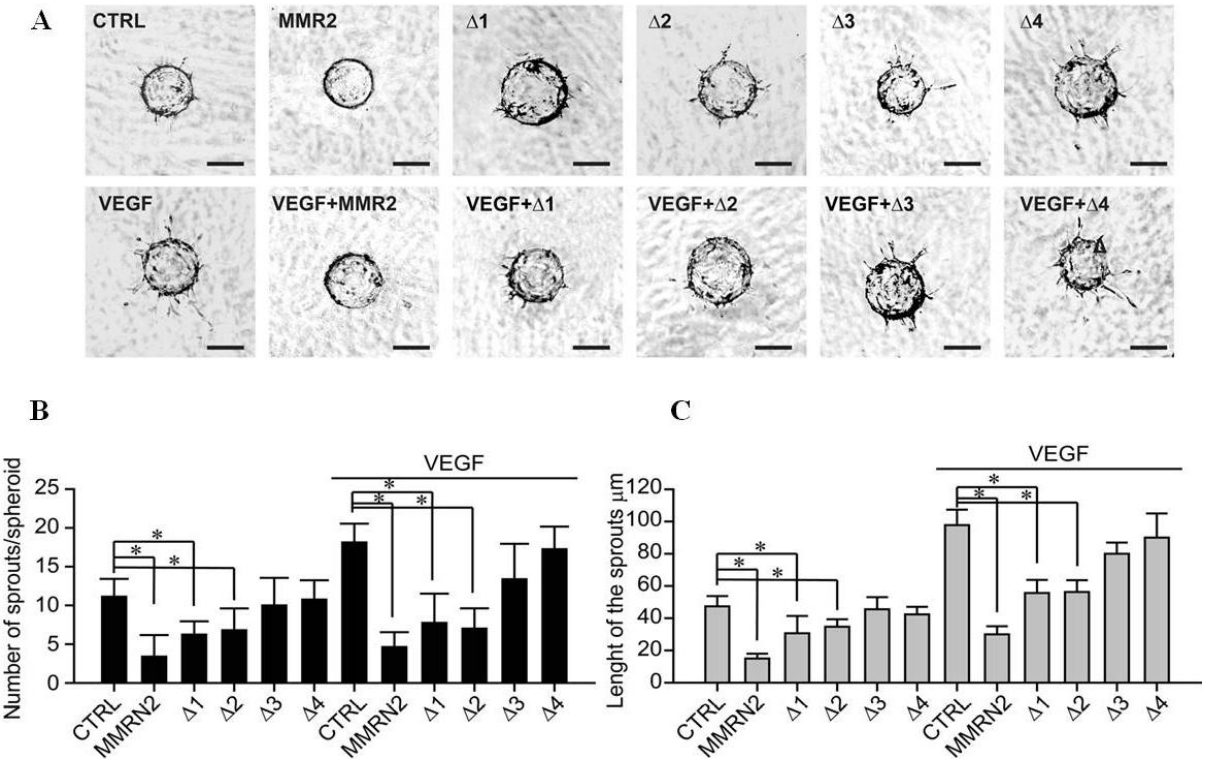

Fig. 5: MMRN2 and its active mutants induce a striking reduction of the vessels' sprouts in a 3D context. (A) Representative images of the spheroid angiogenesis assays performed following coating of HUVEC cells onto cytodex microcarriers end subsequently embedded into a fribrin gel overlaid with normal human dermal fibroblasts (NHDF) to induce EC sprouting. Spheroids were challenged with a 35 nM concentration of MMRN2 and the various deletion mutants in the presence or not of VEGF. Untreated spheroids served as negative control (CTRL); scale bar = 100 µm. **(B)** and **(C)** Graphs representing the evaluation of respectively the number and length of the sprouts of the experiment in D, as obtained with the Image J software; (**P* < 0.001). P values were obtained with the ANOVA one way analysis of variance and graphs represent the mean ± SD obtained from at least three experiments.

Accordingly, we found that the down-modulation of MMRN2 expression significantly increased vessels' sprouting both in terms of number and the length of the sprouts (Fig. 6A to 6C).

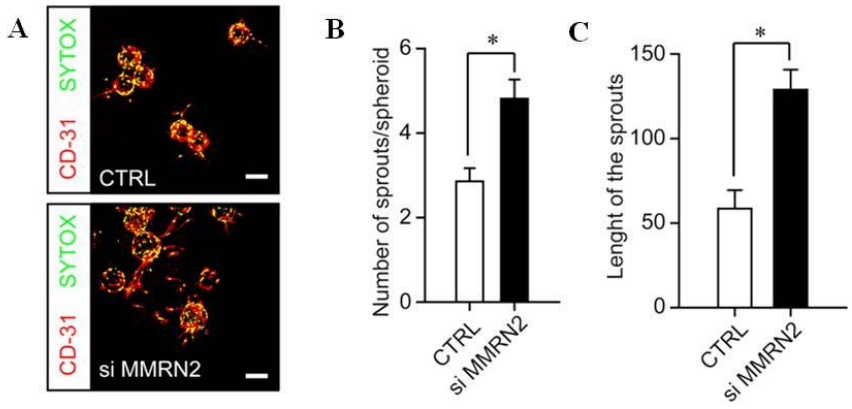

Fig. 6: The down-modulation of MMRN2 expression increased EC sprouting from a spheroid-based test. (A) Representative images of the spheroid angiogenesis assays obtained following coating of HUVEC cells transduced with the control or siMMRN2 adenoviral vectors. Fixed spheroids were stained with α-CD31 (ECs) and SYTOX (nuclei), scale bar = 160 μm. **(B)** and **(C)** Graphs representing respectively the number (*P = 0.006) and the length (*P = 0.009) of the sprouts per spheroid, as assessed by means of the Volocity 3D software. P values were obtained using the Student's t-test and the graphs represent the mean ± SD obtained from at least three independent experiments.

6.4 The MMRN2 active mutant retains the capability to bind VEGF-A_{165}.

Given that we had previously demonstrated that the anti-angiogenic properties of MMRN2 relies, at least in part, on its ability to sequester the 165 isoform of VEGF-A, we wondered if the deletion mutants retained this binding capability**.** To address this question, we performed solid phase analyses in which 0.5 μg of the recombinant MMRN2 and its deletion fragments were immobilized on ELISA plates and incubated with soluble VEGF-A_{165} (100 ng/well). As shown in the Fig. 7A, only Δ1 and Δ2 mutants were able to interact to VEGF-A_{165}, as opposed to the Δ3 and Δ4 mutants. Therefore, since in all experiments carried out, Δ2 mutant turned out to be the shortest fragment resembling the function of the whole molecule, we decided to employ only this mutant for the subsequent experiments. The interaction of VEGF-A_{165} with the Δ2 fragment was further confirmed by BIAcore analysis (Fig. 7B). However, the kD of the interaction (kD = $4.3x10^{-7}$, lower than that previously obtained with the MMRN2 kD = $5x10^{-8}$) was likely underestimated because the immobilization of the Δ2 deletion mutant was not stable as it was released from the chip during the run.

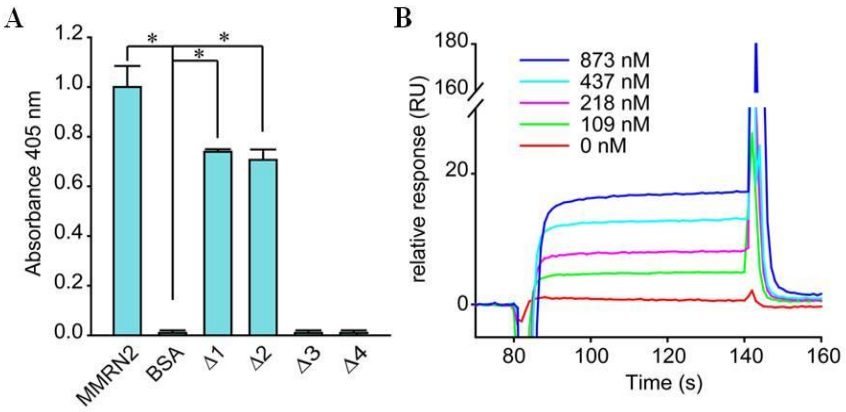

Fig. 7: The Δ2 deletion mutant binds to VEGF-A_{165}. (A) Graph representing the solid phase analysis of the interaction of VEGF-A_{165} with the various deletion mutants indicating that the binding occurs through the region encompassed by the Δ2 fragment. BSA was used as negative control; (*P < 0.001). P values were obtained with the ANOVA one way analysis of variance and graphs represent the mean ± SD obtained from at least three independent experiments. **(B)** Sensogram expressed in resonance units (RU) of the surface plasmon resonance analysis of the interaction of VEGF-A_{165} with the Δ2 deletion mutant, the different concentrations used are indicated and color-coded; kD = 4.3×10^{-7} M.

6.5 The glycosylation of MMRN2 is required for an optimal interaction with VEGF-A_{165}.

Provided that MMRN2 is a glycosylated trimeric molecule able to sequester VEGF-A_{165}, we wondered whether this direct binding occurred through the protein core or the carbohydrate chains. To address this question, we first performed solid phase binding studies in presence or not of heparin, a highly sulfated glycosaminoglycan with an high affinity for VEGF-A_{165}. Interestingly, we found that the interaction of VEGF-A_{165} with MMRN2 was completely abolished in presence of heparin (Fig. 8A). This result suggested that the binding was dependent on the carbohydrate chains and that heparin could compete with the binding. To verify this hypothesis, we next removed the sugar chains from MMRN2 by means of a protein deglycosylation kit. As shown in Fig. 8B, we found that the interaction with VEGF-A_{165} was significantly impaired, despite the binding was not completely abolished. On the other hand, a complete abrogation of the binding was obtained when the cleavage of the carbohydrate chains was achieved under denaturing conditions. Despite this observation, under these conditions we could not rule out the possibility that this effect depended on the lack of the proper folding of the protein. An impaired binding was also observed using the entire molecule and the Δ2 deletion mutant produced under conditions that prevented protein glycosilation. For this purpose, MMRN2 and the Δ2 fragment was expressed in 293-EBNA cells in the presence of tunicamycin and the bands analyzed by Western blotting. The binding of VEGF-A_{165} to the unglycosylated purified proteins were then analyzed through ELISA tests . As shown in Fig. 8C, the absence of carbohydrate chains almost completely abolished the interaction of VEGF-A_{165} to both molecules.

However, also in this case, the Western blot analysis indicated that the treatment with tunicamycin induced also a partial degradation of both recombinant molecules (Fig. 8D). Thus, we concluded that a contribution of the protein core to the interaction with VEGF-A_{165} could not be ruled out.

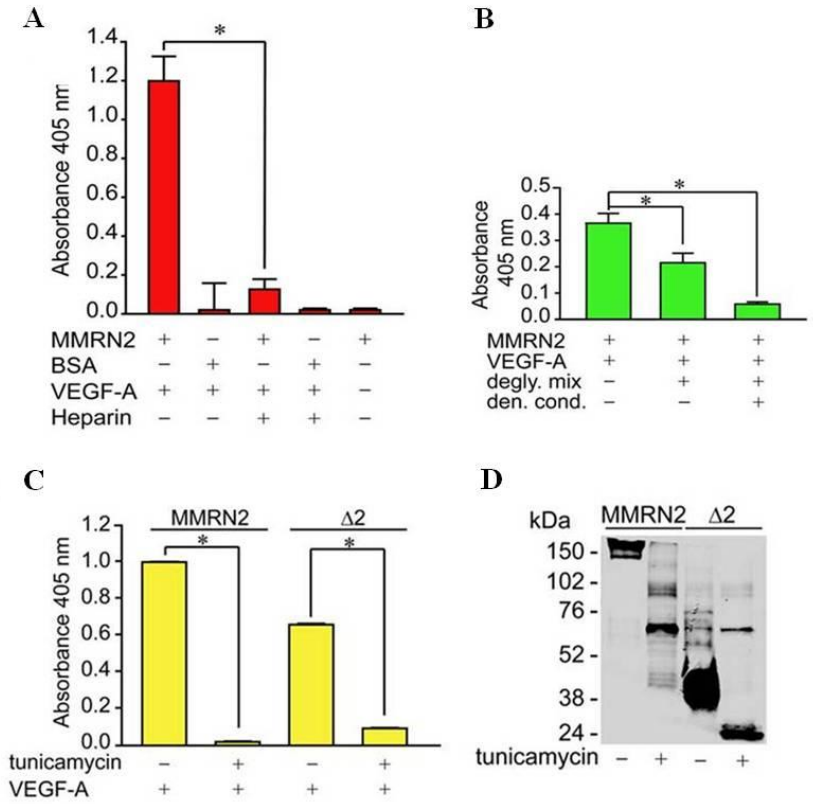

Fig. 8: The binding of VEGF-A_{165} to MMRN2 occurs primarily through the carbohydrate chains (A) Graph representing the solid phase analysis of the interaction of VEGF-A_{165} with MMRN2 in the presence of heparin. BSA was used as negative control; (*P < 0.001). **(B)** Graph representing the solid phase analysis of the MMRN2/VEGF-A_{165} interaction following the cleavage of the carbohydrate chains with the Protein Deglycosylation Mix (degly. mix) under non denaturing or denaturing conditions (den. cond.); (*P < 0.003). **(C)** Graph representing the solid phase analysis of the interaction of MMRN2 and the Δ2 deletion mutant with VEGF-A_{165} with the employment of the recombinant molecules produced in the absence or in the presence of tunicamycin. The absence of the carbohydrate chains completely abolished the interaction; (*P < 0.001). **(D)** Image of the Western blot analysis of recombinant MMRN2 and the Δ2 deletion mutant expressed in the presence or not of tunicamycin. P values were obtained with the ANOVA one way analysis of variance and graphs represent the mean ± SD obtained from at least three experiments.

6.6 The binding of MMRN2 to other VEGF-A isoforms.

To better investigate on the relative contribution of the carbohydrate chains versus the protein core of MMRN2 for the interaction with the cytokine, we assessed the capability of MMRN2 to interact with other VEGF-A isoforms.

To this purpose, VEGF-A_{145} and VEGF-A_{189} displaying high affinity for heparin and VEGF-A_{121} which lacks the heparin binding domain were interrogated for the binding to MMRN2. As shown in Fig. 9A, the VEGF-A_{121} isoform retained the capability to bind to MMRN2 (kD = 2.0×10^{-7} M), despite the interaction was much lower compared to that of VEGF-A_{165}. Thus we concluded that the carbohydrate chains of MMRN2 play an important part in the interaction, despite not exclusive, and that the protein core could be also involved in the interaction. The important contribution of the carbohydrate chains is also suggested by the specific binding detected with VEGF-A_{145} and VEGF-A_{189} (Fig. 9B). Indeed, both isoforms, characterized by a high affinity for heparin, displayed a good interaction with MMRN2, even higher than that observed with VEGF-A_{165} (kD = 2.7×10^{-8} M and kD = 3.0×10^{-9} M, respectively).

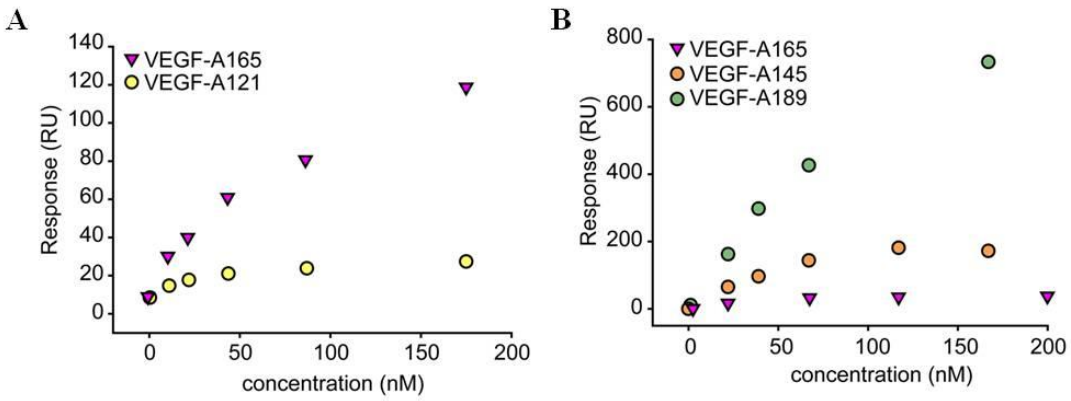

Fig. 9: MMRN2 binds to different VEGF-A isoforms. (A) Dose response plot of the interaction of MMRN2 with VEGF-A_{165} and VEGF-A_{121}, as obtained by surface plasmon resonance. **(B)** Dose response plot of the interaction of MMRN2 with VEGF-A_{165}, VEGF-A_{145} and VEGF-A_{189}, as obtained by surface plasmon resonance.

6.7 MMRN2 binds different VEGF family members.

We have next evaluated whether the binding of MMRN2 was specific for VEGF-A_{165} or if the molecule could also interact with other members of the VEGF family. In particular, the binding of MMRN2 to VEGF-B_{167}, VEGF-C and PlGF-1 was assessed by solid phase analyses. No detectable interaction was found in this experimental setting (Fig. 10A to 10C). The binding to VEGF-D was not verified in this test due to the lack of a good antibody.

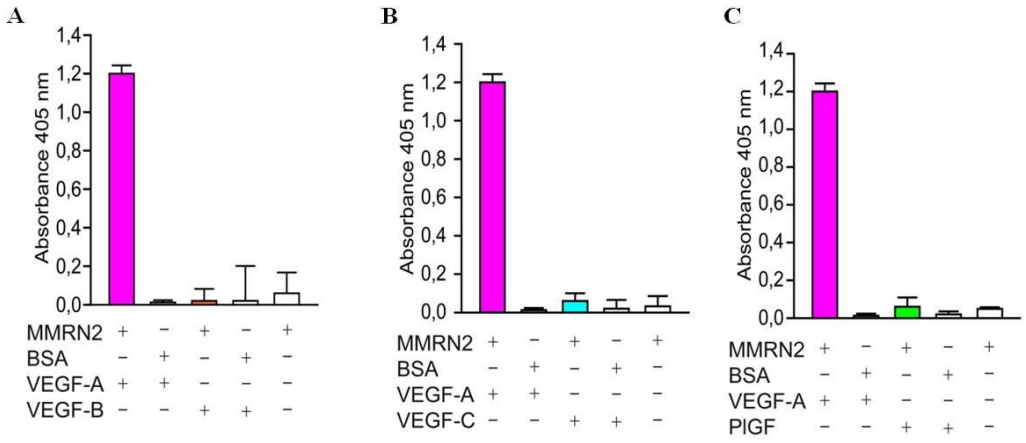

Fig. 10: Analysis of the interaction of MMRN2 with VEGF-B, VEGF-C and PlGF-1 in solid phase analyses (A), **(B), (C),** Graphs representing the solid phase analyses of the interaction of MMRN2 with the VEGF-A family members VEGF-B_{167}, VEGF-C and PlGF-1, respectively.

However, specific interaction was detected through BIAcore analyses (Fig. 11A to 11E), despite it was much lower compared to that of VEGF-A_{165} (kD = 7.5×10^{-7} M, kD = 6.4×10^{-7} M, and kD = 5.6×10^{-7} M). The interaction with VEGF-B_{167} could not be analyzed by plasmon resonance due to non-specific binding of the cytokine to the control flow cell.

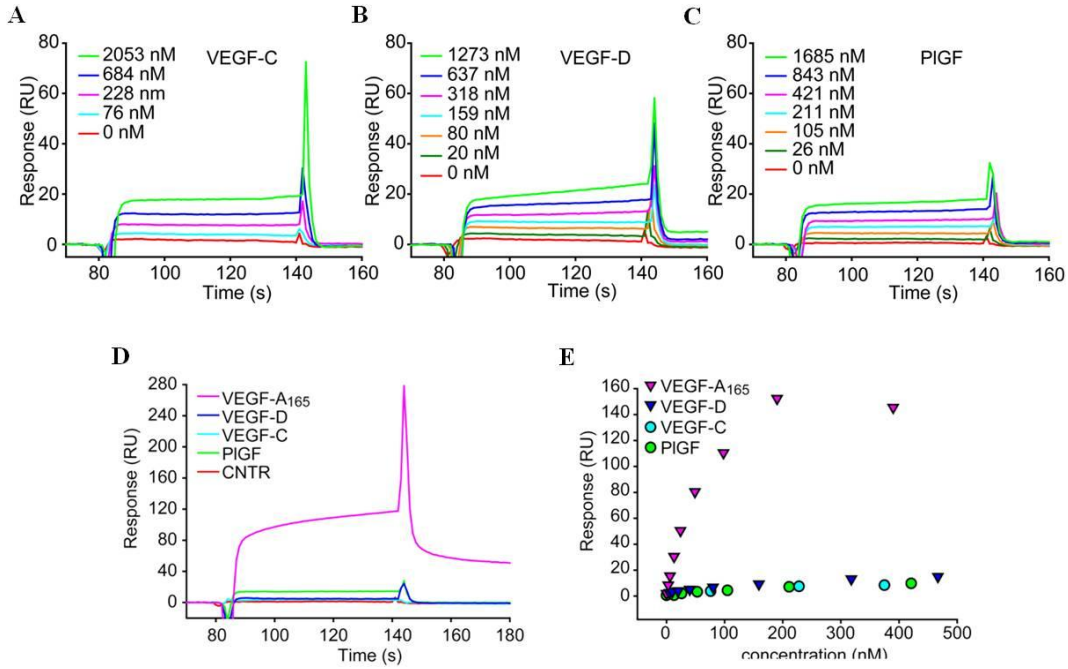

Fig. 11: MMRN2 binds to different VEGF family members (A), (B), (C). Sensograms reporting the binding of VEGF-C, VEGF-D and PlGF-1, as assessed by surface plasmon resonance. **(D)** Sensogram of the the binding at the concentration of 200nM of VEGF-A_{165}, VEGF-C, VEGF-D and PlGF-1 to MMRN2, as assessed by surface plasmon resonance. **(E)** Dose response plot of the interaction of MMRN2 with VEGF-A_{165}, VEGF-C, VEGF-D and PlGF-1, as obtained by surface plasmon resonance. All the experiments were repeated at least three times.

6.8 MMRN2 and its active mutant affect VEGFR2 activation.

We next aimed at better understanding the molecular mechanisms elicited by MMRN2 and its active deletion mutant. In our laboratory we had previously demonstrated that MMRN2 specifically blocked the VEGF-A-driven phosphorylation of VEGFR2 at Y1175 and that this inhibition was accompanied by a significant down-regulation of FAK phosphorylation. In the present study, we wondered whether MMRN2 affected other VEGFR2 tyrosine residues. In particular, given the influence of MMRN2 in EC migration, we analyzed the phosphorylation of residue Y1214 known to be involved in actin remodeling, vascular permeability and cell migration. To this end, HUVEC cells were challenged with MMRN2 (5 µg/ml) in presence or not of $VEGF_{165}$ (15 ng/ml) for 2.5, 5 and 10 minutes. As shown in Fig. 12A to 12C, we found that MMRN2 also inhibits the phosphorylation of VEGFR2 at Y1214 and induces a strong down-modulation of SAPK2/p38 activation. Consistently, the treatment of HUVEC cells for 5 minutes with Δ2 deletion mutant (at the equimolar concentration of 35 nM) inhibited VEGFR2 phosphorylation at both Y1175 (Fig. 12D and 12E) and Y1214 (Fig. 12F and 12G) residues.

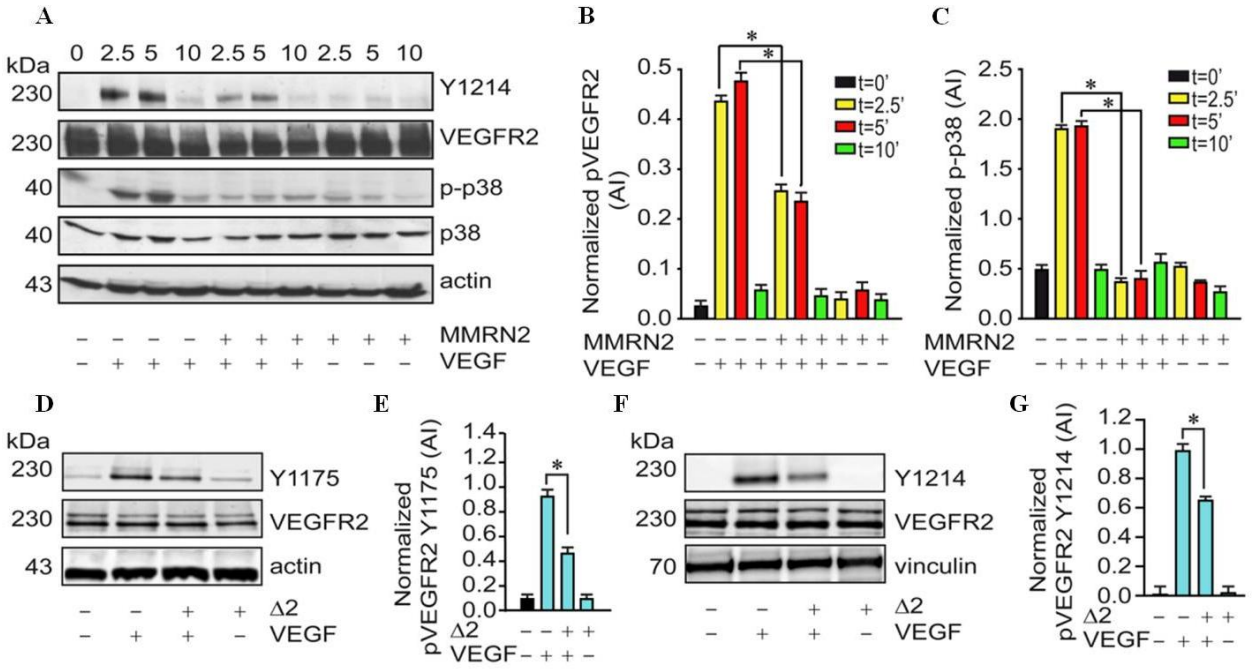

Fig. 12: MMRN2 and the Δ2 deletion mutant impair VEGFR2 activation. (A) Representative image of the Western blot analyses from the lysates of HUVEC cells challenged with MMRN2 in the presence or not of VEGF-A_{165} for different time points (2.5, 5 and 10 min, as indicated). Specific antibodies were used to detect total VEGFR2, pVGEFR2 Y1214, total (p38) and phosphorylated portion of SAPK2/p38 (p-p38). Actin was used as a normalizer of protein loading. **(B)** Graph reporting the quantification, expressed in arbitrary units (AI), of VEGFR2 phosphorylation at Y1214 from the Western blot analyses reported in A, as assessed with the Image J software; (*P < 0.002). **(C)** Graph reporting the quantification, expressed in arbitrary units (AI), of SAPK2/p38 phosphorylation from the Western blot analyses reported in A, as assessed with the Image J software; (*P < 0.001). **(D)** Representative image of the Western blot analyses from the lysates of HUVEC cells challenged for 5 min with the Δ2 deletion mutant in the presence or not of VEGF-A_{165}.

Total VEGFR2 (VEGFR2) and the phosphorylated portion at Y1175 (Y1175) were analyzed with specific antibodies. **(E)** Graph reporting the quantification, expressed in arbitrary units (AI), of VEGFR2 phosphorylation at Y1175 from the Western blot analyses reported in D; (*P = 0.008). **(F)** Representative image of the Western blot analyses from the lysates of HUVEC cells challenged for 5 min with the Δ2 deletion mutant in the presence or not of VEGF-A_{165}. Total VEGFR2 (VEGFR2) and the phosphorylated portion at Y1214 (Y1214) were analyzed with specific antibodies. Vinculin was used as a normalizer of protein loading. **(G)** Graph reporting the quantification, expressed in arbitrary units (AI), of VEGFR2 phosphorylation at Y1214 from the Western blot analyses reported in F; (*P = 0.003). P values were obtained using the Student's t-test to assess the probability of significant differences between two groups and the ANOVA one way analysis for more groups. Graphs represent the mean ± SD obtained from at least three experiments.

6.9 MMRN2 and its active mutant affect the redistribution of VEGFR2 to the EC plasma membrane in response to VEGF-A.

Another important mechanism modulating EC function during the angiogenic process is the regulation of the availability of VEGFR2 receptor at the EC membrane. Thus, to assess whether MMRN2 or its active mutant could also affect this aspect, we treated HUVEC cells with recombinant MMNR2 (5 μg/ml) and an equimolar concentration (35 nM) of the Δ2 active fragment following or not stimulation with VEGF-A_{165} (10 ng/ml) for 20 minutes. The immunofluorescence analyses demonstrated that, in response to VEGF-A_{165} treatment, both molecules induced a significant impairment of redistribution of VEGFR2 at the EC surface (Fig. 13A and 13B).

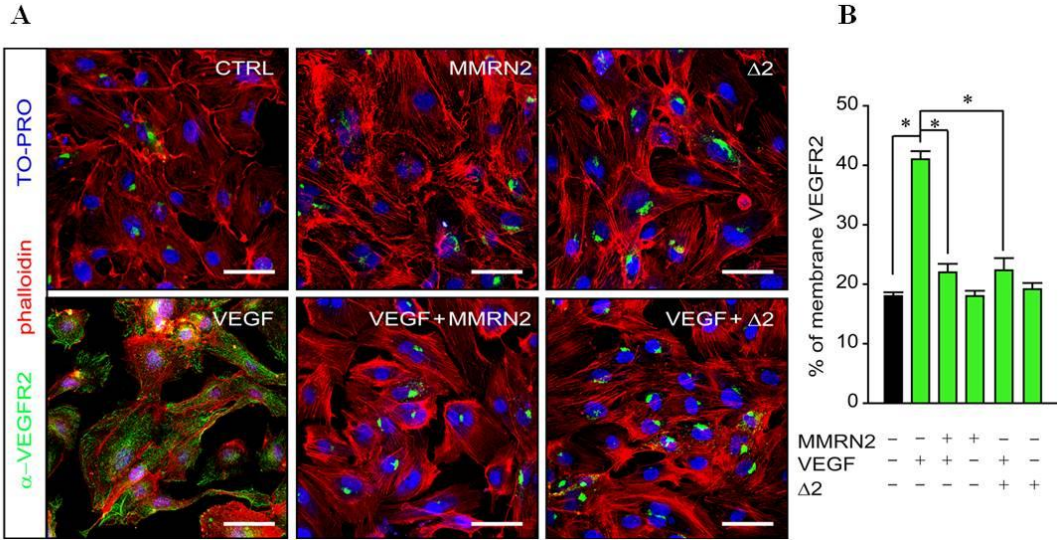

Fig. 13: MMRN2 and the Δ2 deletion mutant impair the redistribution of VEFGR2 at the EC surface. **(A)** Representative images of the immunofluorescence analyses performed to assess VEGFR2 distribution in HUVEC cells challenged with MMRN2 or the Δ2 deletion mutant in the presence or not of VEGF-A_{165}; scale bar = 50 μm.

(B) Graph representing the quantification of the number of cells displaying VEGFR2 staining at the cell surface from the experiment reported in H, at least 10 fields per condition were evaluated; (*P < 0.001). P values were obtained with the ANOVA one way analysis of variance and graphs represent the mean ± SD obtained from at least three experiments

6.10 MMRN2 and its active mutant impair the angiogenic responses in *in vivo* experimental settings.

Given the strong effect exerted by MMRN2 and its active deletion mutant *in vitro,* we hypothesized that they could also play an important anti-angiogenic role *in vivo.* To verify this hypothesis, we performed a Matrigel plug assay in which BALB/c mice were injected under the skin with Matrigel in presence of VEGF-A and basic FGF (bFGF) to induce angiogenesis, whereas Matrigel containing PBS alone served as a negative control. Then, the plugs were treated or not with a concentration of, 35 nM of MMRN2 or the Δ2 recombinant protein to test whether the molecules could affect the development of blood vessels. After 10 days the mice were sacrificed and the excided plugs were analyzed. As shown in Fig. 14A and 14B, MMRN2 and its active deletion mutant reduced the hemoglobin content within Matrigel plugs, as assessed by means of the Drabkin reagent kit. The anti-angiogenic effect of both molecules was further confirmed by hematoxylin and eosin staining performed on the sections obtained from the plugs and the vessels counting (Fig. 14C and 14D).

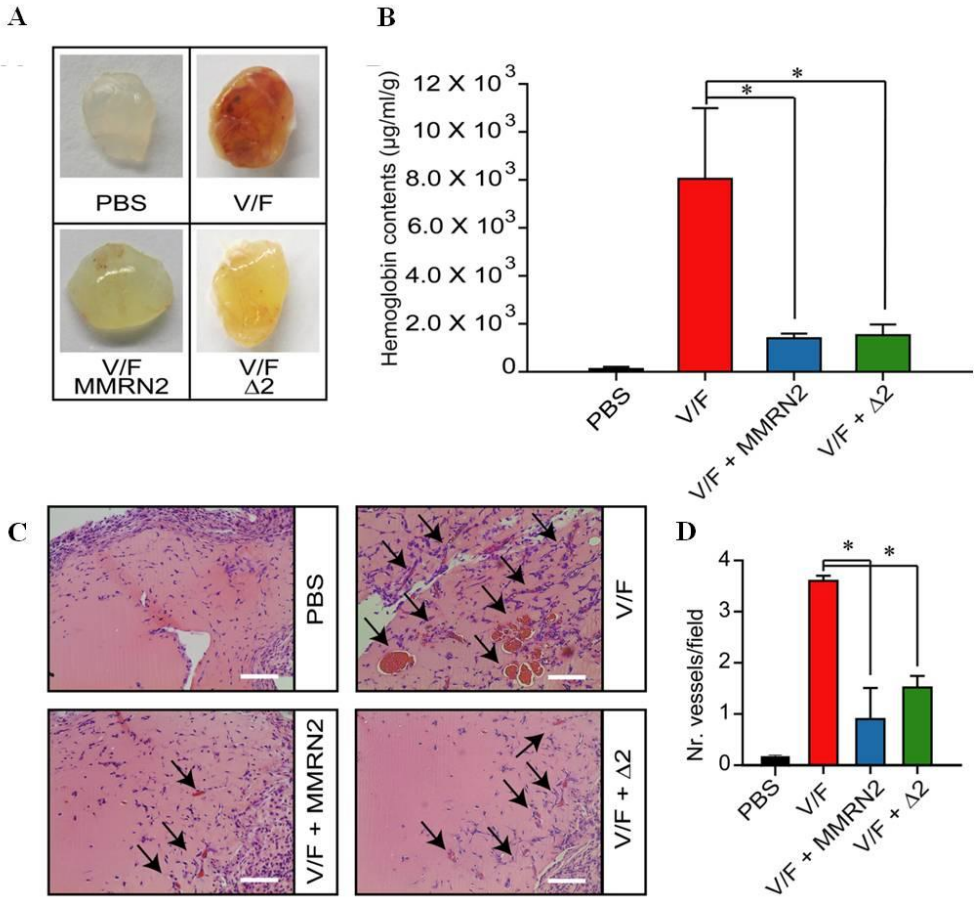

Fig. 14: MMRN2 and the Δ2 deletion mutant impair the development of blood vessels in the *in vivo* Matrigel plug assay. **(A)** Representative images of the plugs explanted from BALB/c mice and challenged with 35 nM of MMRN2 or Δ2 deletion mutant every other day for 10 days, in the presence or not of 50 ng/ml VEGF-A165 and bFGF (V/F). Matrigel plugs were also treated with PBS as control. **(B)** Graph representing the spectrophotometric evaluation of the hemoglobin content within the plugs as assessed by means of the Drabkin's reagent; (*P = 0.004). **(C)** Representative images of the hematoxylin and eosin staining of the Matrigel plugs upon treatment with 35 nM of MMRN2 or the Δ2 deletion mutant, in the presence of 50 ng/ ml VEGF-A165 and bFGF (V/F). The newly formed vessels within the plugs are indicated by an arrow; scale bar = 100 μm. **(D)** Graph representing the evaluation of the number of vessels within the plugs as assessed by counting on at least 10 fields for each point; (*P < 0.001). P values were obtained with the ANOVA one way analysis of variance and graphs represent the mean ± SD obtained from at least three experiments.

6.11 MMRN2 and its active mutant halt the *in vivo* tumor growth and tumor angiogenesis.

Next we verified whether the Δ2 active mutant could affect tumor growth and tumor associated angiogenesis, as demonstrated for the entire molecule (Lorenzon E. et al., 2012). For this purpose we generated HT-1080 cells ectopically expressing the Δ2 deletion mutant. Then, the Δ2 over-expressing cells were implanted in the right flank of 10 nude mice, whereas in the left flank the mice were injected with mock transfected cells. In parallel, another group of mice were injected in the right flank with HT-1080 cells over-expressing MMRN2 and in the left flank with mock transfected cells. Tumor growth was monitored and the sizes measured. As shown in Fig. 15A and 15B, in presence of both MMRN2 and the active fragment a strong inhibition of tumor growth was observed.

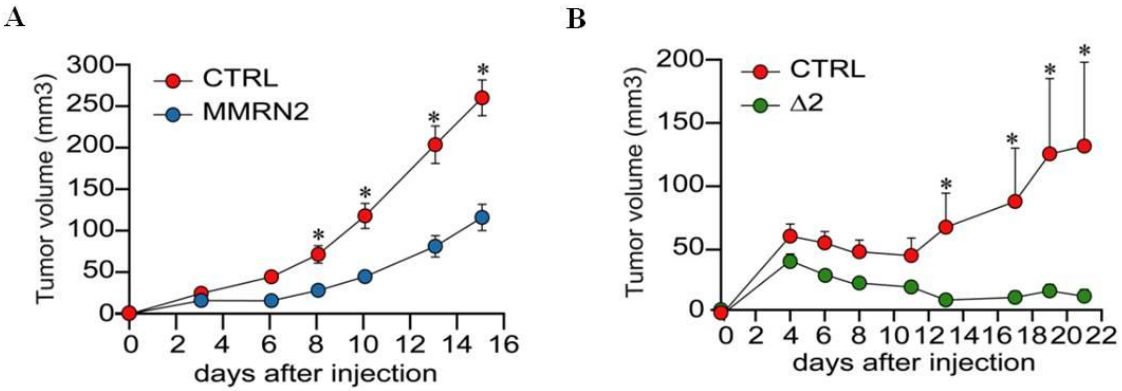

Fig. 15: The over-expression of MMRN2 and the Δ2 deletion mutant is associated with a decreased tumor growth. (A) Graph reporting the measurements of the tumor volumes following the injection of mock-transfected HT1080 cells (CTRL, left flank) or MMRN2 over-expressing cells (MMRN2, right flank), as evaluated by means of a caliper; (*P < 0.001). **(B)** Graph reporting the measurements of the tumor volumes following the injection of mock-transfected HT1080 cells (CTRL, left flank) or Δ2 deletion over-expressing cells (Δ2, right flank), as evaluated by means of a caliper; (*P < 0.001). P values were obtained using the Student's t-test and the graphs represent the mean ± SD obtained from at least three experiments.

As demonstrated for the whole molecule, the anti-tumorigenic effect of Δ2 deletion mutant was likely indirect since the fragment did not alter the proliferation and the apoptotic rate of the tumor cells *in vitro*. In fact, the proliferation of Δ2 over-expressing cells at 24, 48, 72 and 96 hours following seeding on 96-well plates, was comparable to that of mock-transfected cells (Fig. 16A). Furthermore, also the apoptotic rate of HUVEC cells transfected with Δ2 deletion mutant construct was comparable to that of cells transfected with the empty vector, as assessed by TUNEL assay after 48 hours of incubation (Fig. 16B).

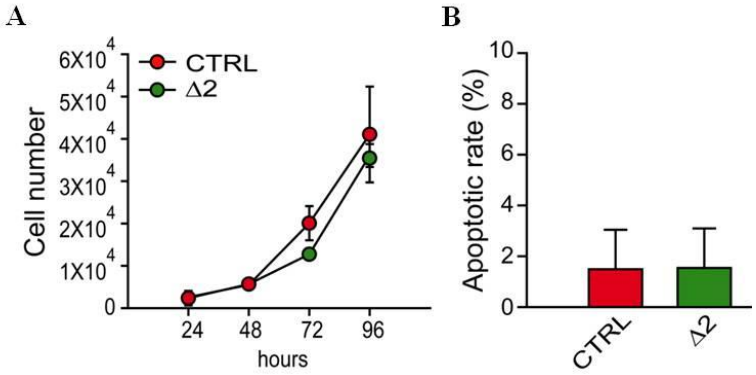

Fig. 16: MMRN2 and the Δ2 deletion mutant did not affect the proliferation or apoptotic rate of HT1080 cells *in vitro*. (A) Graph reporting the growth curve of mock- or Δ2-transfected cells after 24, 48 72 and 96 hours of incubation, as assessed by counting. (**B**) Graph reporting the similar % of apoptotic cells following transfection of HT1080 cells with the empty vector (CTRL) or Δ2 deletion mutant construct, as assessed by TUNEL assay. P values were obtained with the ANOVA one way analysis of variance and graphs represent the mean ± SD obtained from at least three experiments.

Since the originated data indicated that the strong inhibition of tumor growth observed was not associated to a direct action of MMRN2 or its active mutant on cancer cells, we verified if this effect was due to a reduced intra-tumoral angiogenesis. In order to verify this hypothesis, we injected the animals with AngioSense 750EX and verified *in vivo* that both the whole molecule and the Δ2 deletion mutant strongly reduced the formation of vessels within the tumors (Fig. 17A to 17D).

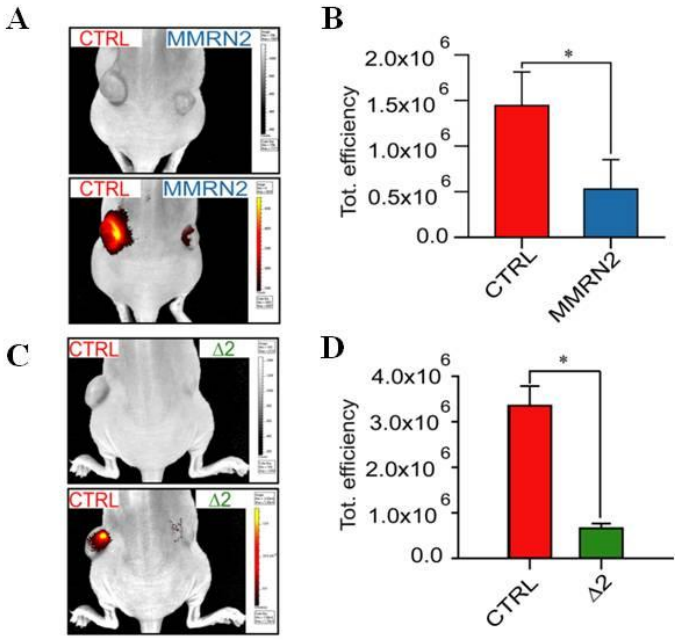

Fig. 17: The over-expression of MMRN2 and Δ2 deletion mutant is associated with an impaired intratumoral vascularization. (A). Representative image of the *in vivo* Imaging analyses following injection of AngioSense® 750EX in nude mice carrying control tumors (CTRL, left flank) or MMRN2 over-expressing tumors (MMRN2, right flank). Top image mouse photograph showing the decreased growth of the MMRN2-ectopically expressing tumors, bottom image overlay of the photograph with the fluorescent signal of the AngioSense® 750EX probe. **(B)** Graph reporting the analysis of the fluorescent signals from mock (CTRL) and MMRN2 over-expressing tumors, as assessed with the dedicated software of the IVIS® Lumina instrument; (**P* = 0.03). **(C)** Representative image of the *in vivo* Imaging analyses following injection of AngioSense® 750EX in nude mice carrying the control (CTRL, left flank) or the Δ2 deletion over-expressing (Δ2, right flank) tumors. Top image mouse photograph showing the decreased tumor growth of Δ2-ectopically expressing tumors, bottom image overlay of the photograph with the fluorescent signal of the AngioSense® 750EX probe. **(D)** Graph reporting the analysis of the fluorescent signals from the mock (CTRL) and the Δ2 deletion over-expressing tumors, as assessed with the dedicated software of the IVIS® Lumina instrument; (**P* = 0.004). P values were obtained using the Student's t-test and graphs represent the mean ± SD obtained from at least three experiments

This finding was further confirmed by immunofluorescence analyses performed on sections obtained from the excised tumors. The cryosections were stained with the anti-mouse CD31 monoclonal antibody to specifically detect the blood vessels and vessel density was assessed by counting five independent fields. As shown in Fig. 18A and 18B, a striking reduction of vessel density was observed in MMRN2 and Δ2 over-expressing tumors, as compared to the control counterpart.

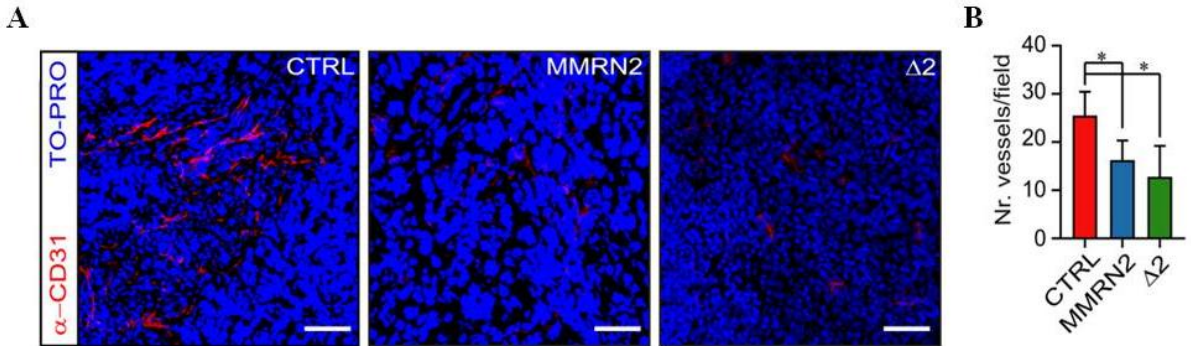

Fig. 18: The MMRN2 and Δ2 over-expressing tumors display an impaired vascular density. (A) Representative images of the immunofluorescent analyses performed on tumor sections from mock-, MMRN2- and Δ2-tumors (CTRL, MMRN2 and Δ2, respectively). Blood vessels were stained through an anti-CD31 antibody (α-CD31) and nuclei with TO-PRO; scale bar = 70 μm. **(B)** Graph reporting the analysis of the number of vessels per field as assessed by counting in at least 10 fields from the mock, MMRN2 and Δ2 tumor sections; (*P < 0.001). P values from were obtained with the ANOVA one way analysis of variance and graphs represent the mean ± SD obtained from at least three experiments.

Finally, to evaluate whether the decrease vessel density was associated with a modification of tumor microenvironment, such as the formation of hypoxic areas, we analyzed the expression of the Hypoxia-Inducible Factor-1 (HIF-1α), which is elicited when the oxygen content within the tissues decreases considerably. The qPCR analyses indicated that the MMRN2 and the Δ2 deletion over-expressing tumors were characterized by an increased expression of HIF-1α and thus were likely more hypoxic compared to the control tumors (Fig.19).

In conclusion, in the first part of this thesis we identify the region of MMRN2 responsible for the binding to VEGF-A_{165}, demonstrate that it primarily involves the carbohydrate chains and verify the angiostatic activity both *in vitro* and *in vivo*.

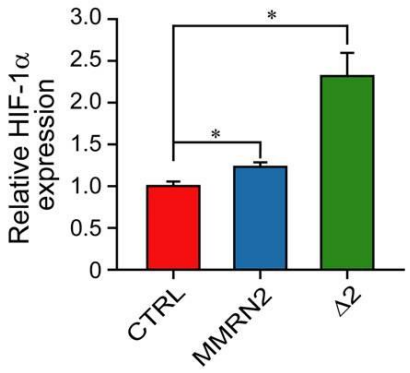

Fig. 19: The MMRN2 and Δ2 over-expressing tumors display an increased expression of HIF-1α. Graph reporting the qPCR analysis of HIF-1α expression in control (CTRL) or MMRN2/Δ2 deletion over-expressing tumors (*P < 0.001). P values were obtained with the ANOVA one way analysis of variance and graphs represent the mean ± SD obtained from at least three experiments.

6.12 Role of MMRN2 in vascular homeostasis.

The data reported above further highlighted the key role of MMRN2 as an angiostatic molecule and prompted us to investigate another important aspect in which the protein is likely implicated: the vascular homeostasis. Indeed, given that MMRN2 is deposited in tight juxtaposition with ECs during the late stages of vascular development and is present in all the blood vessels in adulthood, we hypothesized that the molecule could also be involved in the regulation of blood vessel stability and homeostasis. Hence, the second part of my PhD project was dedicated to investigate this important aspect and the preliminary data that were generated are reported below.

6.13 The deposition and organization of MMRN2 by ECs is boosted by the presence of pericytes.

In order to assess how MMRN2 is secreted over-time by ECs and organized along the endothelium, HUVEC cells were seeded on coverslips and allowed to grow for 1, 3 and 5 days.

We next performed the immunofluoresce analyses using a specific affinity purified anti-MMRN2 polyclonal antibody that we have generated, which demonstrated that the deposition of MMRN2 increased over time as well as its organization into fibrils (Fig. 20A). Interestingly, when the HUVEC cells were put in co-colture with human brain vascular pericytes (HBVP) we observed a strong increase of MMRN2 secretion and deposition compared to the condition in which the cells were seeded alone (Fig. 20B).

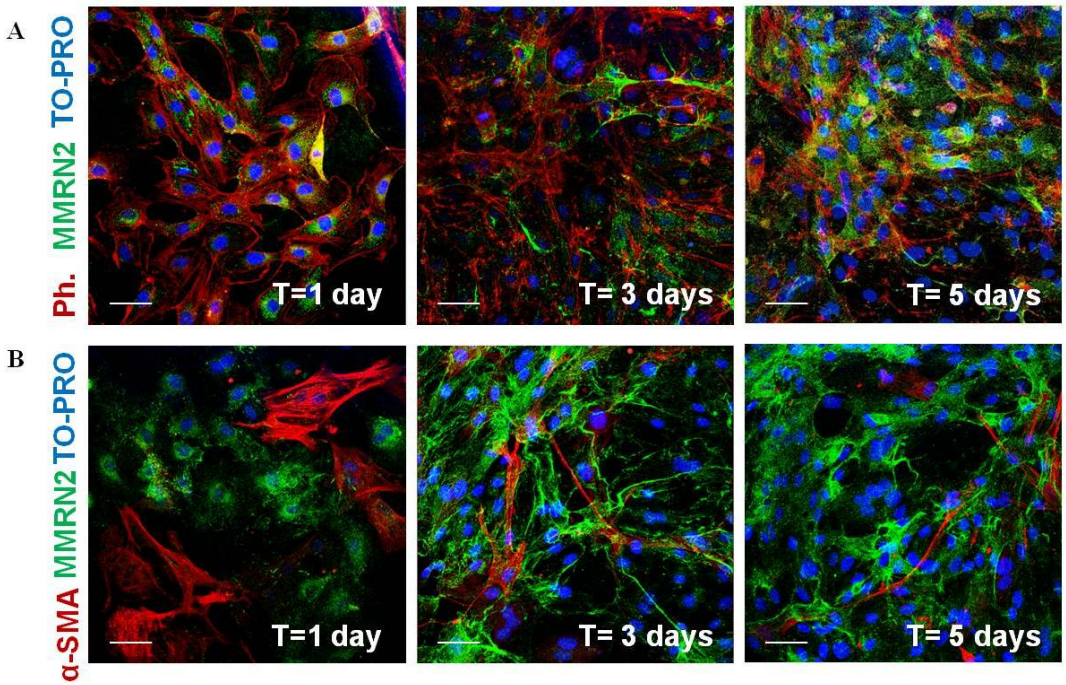

Fig. 20: Pericytes positively affect the over time deposition of MMRN2 by ECs. (A) HUVEC cells were allowed to grow alone for 1, 3 and 5 days, then fixed and processed for immunofluoresce analysis.

The coverslips were stained with phalloidin (Ph) to highlight the actin cytoskeleton and the anti-MMRN2 antibody; nuclei were stained with TO-PRO. **(B)** Immunofluorescence analysis of HUVEC cells in co-culture with pericytes (HBVP) at different times points. Nuclei were stained with TO-PRO, pericytes were stained with the α-SMA antibody and MMRN2 with the specific affinity-purified polyclonal antibody. Scale bar = 50μm.

To further verify if pericytes could influence MMRN2 deposition and organization, HUVEC cells were seeded alone or in co-colture with pericytes at different ratio. As shown in Fig. 21, not only the deposition of MMRN2 but also its organization into fibrils was striking enhanced in presence of an increasing number of pericytes in culture. Thus, we concluded that MMRN2 is strongly influenced by pericytes but the mechanisms responsible for this effect are still not clear for us.

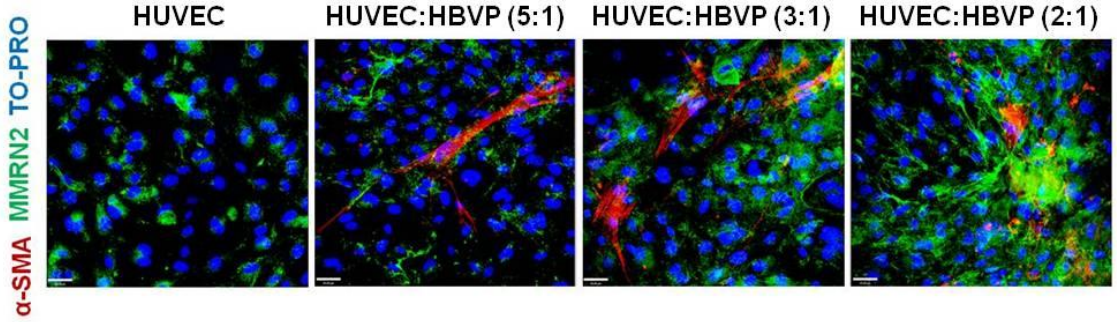

Fig. 21: An high concentration of pericytes boosts MMRN2 deposition and organization. Immunofluorescence analyses of HUVEC cells seeded, for 5 days, alone or in co-colture with pericytes at different ratios (5:1, 3:1, 2:1). The cells were stained with an α-SMA antibody to detect pericytes and the anti-MMRN2 affinity-purified polyclonal antibody. Nuclei were stained with TO-PRO. Scale bar = 35μm

6.14 MMRN2 represents a substrate for pericytes' adhesion.

Next, given the putative role of pericytes in MMRN2 deposition we wondered if the molecule could represent an adhesion substrate for these cells. To address this question, we performed an adhesion assay in which human pericytes were seeded on plates coated with MMRN2 or collagen type I, used as a positive control. After the incubation, the cells were stained with crystal violet and the adhesion was assessed measuring the Absorbance at 560 nm (Fig. 22A and 22B). Our results indicated that the adhesion of HBVP to MMRN2 was comparable to that detected on collagen type I. This finding was further confirmed by monitoring over-time the adhesion of pericytes to collagen type I and MMRN2 by means of the xCELLigence system (Fig. 22C).

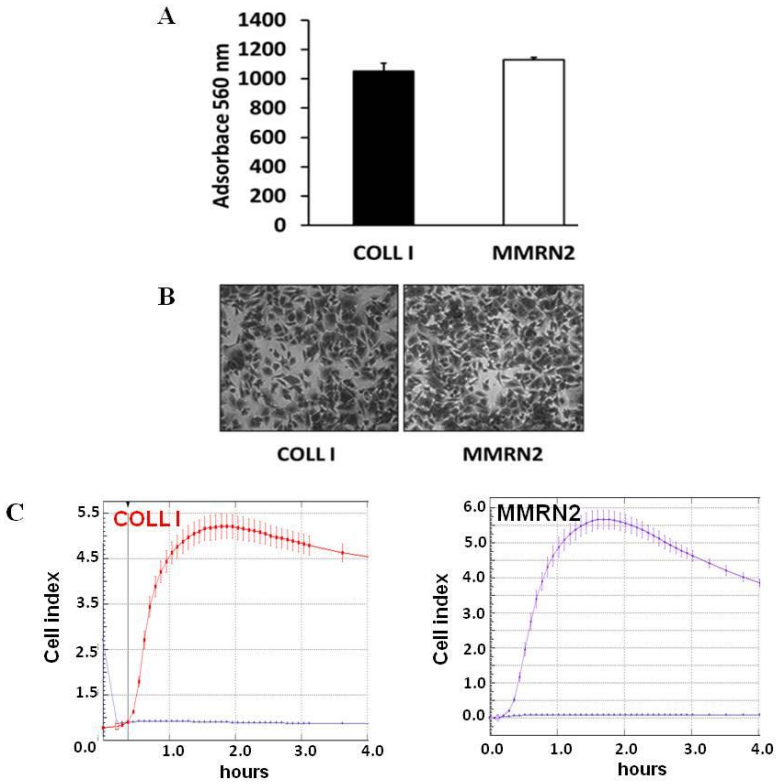

Fig. 22: MMRN2 represents a substrate for the adhesion of pericytes. **(A)** Graph representing the absorbance of Crystal Violet-stained cells following adhesion of HBVP plated on collagen type I (COLL I) or MMRN2. **(B)** Representative image of the adhesion assay reported in A **(C)** Evaluation of the pericyte adhesion to collagen type I or MMRN2 by means of the xCELLigence system.

Interestingly, not only the secretion and organization of MMRN2 seems to be affected by pericytes, of which MMRN2 is a significant adhesion substrate, but it's also likely that an initial deposition of MMRN2 could serve to achieve an optimal recruitment of pericytes. This hypothesis was suggested by the immunofluorescence analyses performed on the whole mounted retinas obtained from wild type (WT) and MMRN2$^{-/-}$ C57BL/6 mice. In fact, as shown in Fig. 23A and 23B not only the retinas from the MMRN2 knock-out mice display an increased vascular density compared to that detected in wild type mice, but they also display an impaired pericyte coverage.

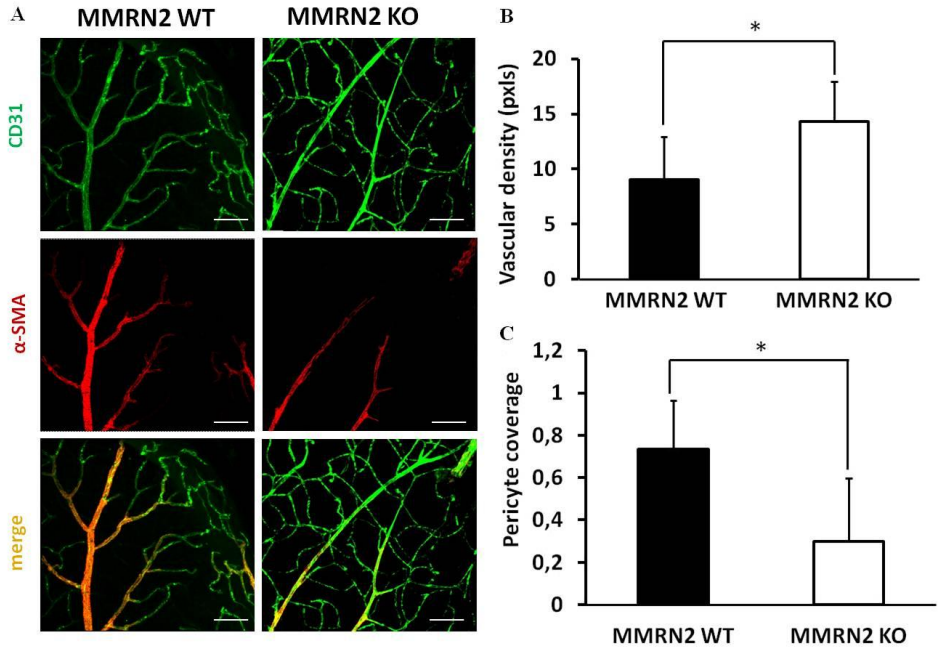

Fig. 23: MMRN2 KO mice display a significant impairment of the pericyte coverage of the retinal vessels. (A) Immunofluorescence analysis of whole mounted retinas from wild type (WT) and MMRN2$^{-/-}$ C57BL/6 mice stained with the anti-CD31 (vessels) and the anti-α-SMA (pericytes). (B) Graph representing the quantitative analysis of the vascular density (*P < 0.05), as obtained by means of the Image Tool software. (C) Graph representing the quantification of the co-localization of the anti-CD31 and the anti-a-SMA staining obtained from the immunofluorescence analysis (*P < 0.05). P values were obtained using the Student's t-test and graphs represent the mean ± SD obtained from at least three experiments.

6.15 MMRN2 affects vascular permeability.

Given the strategic deposition of MMRN2 in close proximity with the EC' plasma membrane, we also questioned whether the protein could affect other important mechanisms characterizing the biology of ECs, such as those determining the formation and integrity of the EC' monolayer.
To address this hypotesis, we modulated the expression of MMRN2 in HUVEC cells and tested the effect on vascular permeability. To this end, HUVEC cells were transduced with MMRN2 siRNA (Ad siRNA) adenoviral or empty vector (Ad NEG), seeded on collagen type I-coated Transwell filters in 24-well dishes and grown for 5 days until they had reached confluency. Subsequently, the functionality of the EC barrier was assessed through the addition of FITC-Dextran on the top of the monolayer. The permeability of the monolayer in terms of FITC-Dextran leakage was measured by evaluating the presence of the compound at the wells' bottom. As shown in Fig. 24, the down-modulation of MMRN2 expression in ECs leads to a significant increase of vascular permeability in an *in vitro* experimental setting.

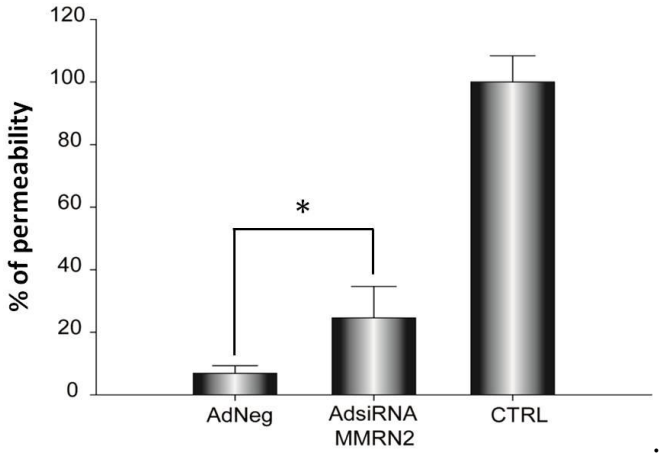

Fig. 24: MMRN2 is involved in the regulation of vascular permeability. Graph reporting the analysis of the % of the permeability of the HUVEC cells' monolayers following transduction with the MMRN2 siRNA (Ad siRNA) adenoviral or the control vector (Ad NEG). Transwells' membranes coated with collagen type I without ECs served as a control (CTRL). Its represents the 100% of vascular permeability respect to which was calculated the percentage of vascular permeability of the other two conditions. P values were obtained using the Student's t-test and graphs represent the mean ± SD obtained from at least three experiments.

This outcome led to the hypothesis that MMRN2 could be involved in the regulation of the formation of the cell-cell contacts. To verify this hypothesis we analyzed the distribution and expression of some proteins localized at the adherens and tight junctions following the down-modulation of MMRN2 expression. Thus, HUVEC cells were transduced with the control or MMRN2 siRNA adenoviral vectors and the distribution/expression of the adherens junction protein VE-cadherin as well as the tight junction associated proteins zona-occludens-1 (ZO-1) and occludin (OCLN) was assessed by immunofluorescence. From these analyses we could conclude that the silencing of MMRN2 induced a significant alteration of OCLN and ZO-1 distribution along the tight junctions of ECs, whereas the distribution of VE-cadherin was not altered (Fig. 25A). Simultaneously, the expression of these molecules was analyzed by Western blotting under the same conditions. These analyses indicated that overall the total amount of OCLN and ZO-1 does not change upon modulation of MMRN2 expression (Fig. 25B). Thus, we concluded that the silencing of MMRN2 may compromise endothelial barrier function disturbing the localization but not the expression of these two tight junction's molecules.

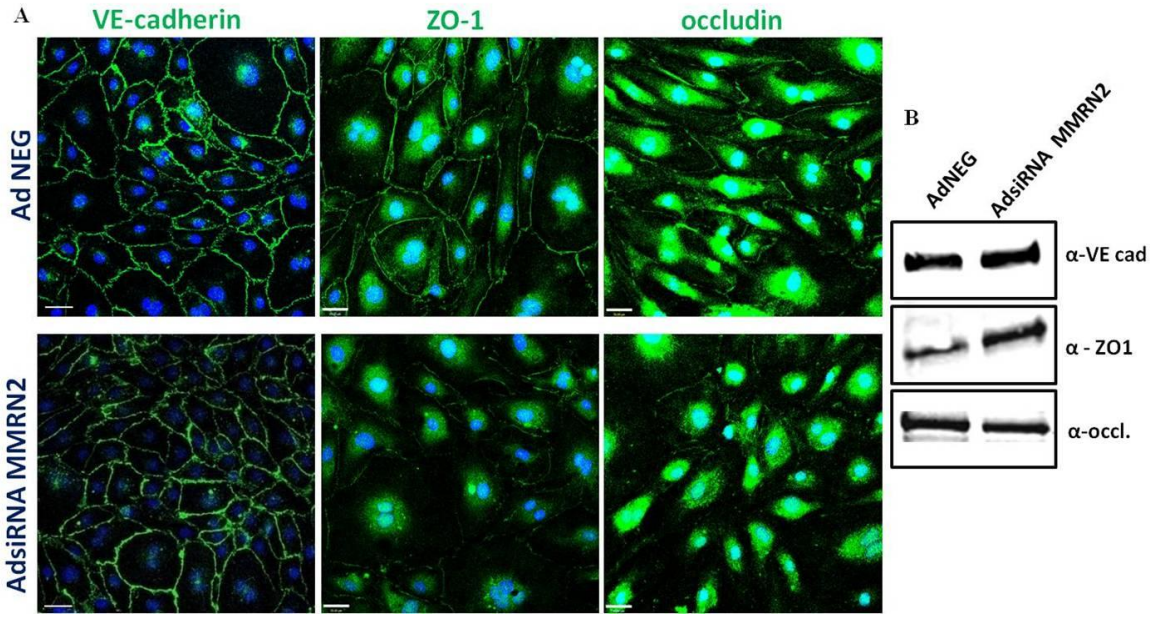

Fig. 25: Analysis of adherens and tight junctions following the modulation of MMRN2 expression. (A) Immunofluorescence analysis of HUVEC cells transducted with MMRN2 siRNA (Ad siRNA) adenoviral or control vector (Ad NEG) and stained with specific antibodies detecting VE-cadherin, OCLN or ZO-1 (zona occludens-1). Nuclei were stained with TO-PRO. Scale bar = 35µm. **(B)** Representative image of the Western blot analyses using lysates of HUVEC cells transducted with the MMRN2 siRNA (Ad siRNA) or control (Ad NEG) adenoviral vectors and grown till confluence was reached. Specific antibodies were used to detect VE-cadherin, OCLN and ZO-1.

Finally, given the promising role of MMRN2 in the regulation of vascular permeability, we decided to corroborate these results *in vivo*. To this end, we employed the MMRN2 knockout mouse model and analyzed the vascular permeability in response to VEGF-A treatment. In particular, wild type and MMRN2$^{-/-}$ mice were intradermically injected in the ear with 50 ng/ml of VEGF-A or the corresponding volume of vehicle. Next, the mice received a retro-orbital injection of FITC-Dextran. The mice were then sacrificed and the ears collected, fixed and analyzed by a stereo microscope. In accordance with the *in vitro* results, the MMRN2 deficient mice displayed an increased vascular leakage compared to that observed in WT mice.

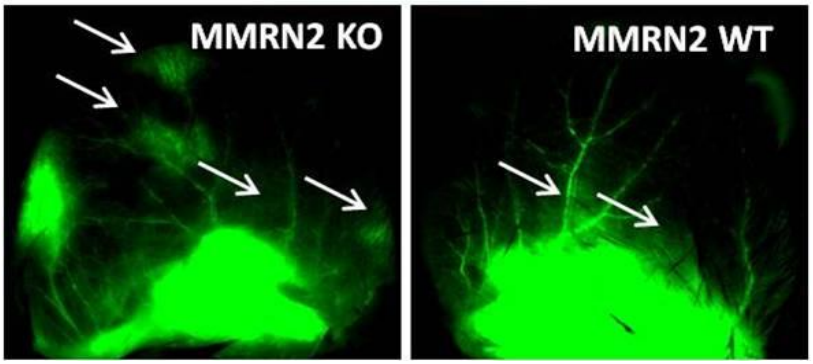

Fig. 25: MMRN2 deficient mice display an increased vascular permeability. WT and MMRN2$^{-/-}$ C57BL/6 mice were examined for vascular leakeage after intradermal injection of vehicle (PBS) or VEGF (50 ng/ml) in mouse ear followed by retrorbital injection of 70-kD FITC-Dextran. The vessel leakage permeability (white arrows) was assessed through immunofluoresce analyses by means of a stereo microscope.

Taken together, the preliminary results presented in the second part of this thesis suggest that MMRN2 may play an important role in the regulation of vascular homeostasis. Despite these evidences, further analyses are required to better define how MMRN2 regulates blood vessels' stability and permeability and to verify if this could influence tumor progression depending on the levels of the expression of the molecule.

7. DISCUSSION

The first part of my investigation was dedicated to further dissect the role of MMRN2 in the regulation of VEGF/VEGFR2 signaling pathway, the interaction with other members of the VEGF family and the effects on angiogenesis and tumor growth. The results obtained have been recently published by Oncotarget (Colladel R. et al., 2015). In particular, in this study, we corroborated the angiostatic function of MMRN2 and identified the active region responsible for these effects. Unlike EMILIN2, another member of the EDEN family, that simultaneously inhibits tumor growth by activating apoptosis (Mongiat M. et al., 2010; Marastoni S. et al., 2014) and induces the new vessel formation (Mongiat M. et al., 2010), the localization and the function of MMRN2 is specific and well characterized. MMRN2 instead plays a negative role in new blood vessel development, primarily acting through the inhibition of EC motility. This effect depends, at least in part, on its binding to VEGF-$A_{165,}$ and the sequestration of the ligand, one of the major cytokines promoting angiogenesis, leads to a down-regulation of VEGFR2.

This investigation led to the discovery of a discrete portion of the molecule named Δ2 and located in the central coiled-coil region of the glycoprotein. By means of *in vitro* and *in vivo* tests we demonstrated that this fragment recapitulated all the effects exerted by the entire molecule. These results were compelling and were corroborated in an wide number of tests, including migration, proliferation, TUNEL assays, tubuligenesis on matrigel, as well as spheroid-based tests.
A further discovery from these analyses indicated that the binding of MMRN2 and its active fragment to VEGF-A_{165} primarily occurs through the carbohydrate chains, since their enzymatic removal partially halted the interaction. Nonetheless, these examinations indicated that also the protein core was involved in the interaction, despite with a minor contribution. This conclusion was principally drawn by two observations. First, a specific binding, even if lower compared to that of VEGF-A_{165}, was as well detected with the VEGF-A_{121} isoform, which lacks the heparin binding domain. Second, while testing of the binding of MMRN2 to other VEGF-A isoforms, we found that the glycoprotein interacted also with VEGF-A_{145} and VEGF-A_{189}. These two isoforms are characterized by a higher affinity for heparin (Vempati P. et al 2014) if compared to that of VEGF-A_{165}, and accordingly, their affinity of the binding to MMRN2 was higher than that detected for VEGF-A_{165}.

The BIAcore analyses in order to determine if the interaction was specific for VEGF-A and the relative isoforms or it could be extended to other family members, indicated that MMRN2 displays a specific binding also with VEGF-C, VEGF-D, and PlGF-1, despite the affinity was weaker compared to that of VEGF-A_{165}. Given the major role of the carbohydrate chains of MMRN2 in the interaction with these growth factors, it is possible that the low binding affinity for VEGF-C, VEGF-D, and PlGF-1 may depend on a different arrangement of the basic residues involved in the interaction with the carbohydrates (Chiodelli P. et al., 2015). Thus, from these analyses we may assume that MMRN2 could bind many cytokines halting angiogenesis and affecting the tumor microenvironment through different mechanisms.
The striking biological effect obtained for Δ2 deletion mutant and the high number of putative glycosilated sites, 5 out of a total of 11 distributed along the whole molecule, led us to suppose that most of the VEGF-A is sequestered within this region.

An attempt to further dissect the functional region was pursued but none of the three smaller constructs generated could be secreted by 293-EBNA cells (data not shown). Since this fragment is characterized by alternated coiled-coil regions, it is possible that the smaller constructs did affect the local folding and prevent a proper trimerization process of the molecule, thus leading to protein degradation.

Subsequently, my interest focused on better clarifying the mechanisms by which MMRN2 and its active mutant could impair EC motility. In our laboratory we had previously shown that MMRN2 down-regulated the phosphorylation of VEGFR2 at Tyr1175 through the sequestration of VEGF-A_{165} (Lorenzon E. et al., 2012). In this study we demonstrated that also Δ2 active mutant retains this function. Next, we further dissected the role of MMRN2 and its Δ2 deletion mutant in affecting VEGFR2 activation analyzing other important phosphorylation sites of the receptor. We found that, through the binding to VEGF-A_{165}, both MMRN2 and the active fragment led to the down-modulation of the phosphorylation of the receptor at Tyr1214 and, in turn, to a strong reduction of the activation of the SAPK2/p38 pathway. This result further reinforces our findings indicating that MMRN2 mostly impairs EC motility, in fact Tyr1214 is a key site whose phosphorylation regulates cell migration, actin remodeling and vascular permeability (Lamalice L. et al., 2004).

Furthermore, in this study we also demonstrated an additional mechanism through which MMRN2 negatively affects VEGFR2 activation. This involves the intracellular confinement of the receptor in the Golgi apparatus which is enhanced in the presence of MMRN2, thus reducing the availability of the receptor at the cell surface. It is known that the binding of VEGF-A to VEGFR2 at the plasma membrane induces the exit of intracellular VEGFR2 from the Golgi apparatus en route to the plasma membrane (Manickam V. et al., 2011). The treatment of ECs with MMRN2 or its Δ2 deletion mutant did not lead to a detectable decrease of the total levels of expression of VEGFR2, as indicated by the Western blot analyses. Thus, it is likely that the impaired recruitment of the receptor at the cell surface may strictly depend on the sequestration of VEGF-A by MMRN2/Δ2, and thus on its decreased availability for receptor engagement. These findings further strengthen the role of MMRN2/Δ2 deletion mutant in negatively regulating EC activation by impinging on the VEGF-A/VEGFR2 signaling axis.

It was recently published that the interaction of MMRN2 to CLEC14A, a single-pass transmembrane glycoprotein specifically expressed by ECs, induces the inhibition of sprouting angiogenesis and tumor growth (Noy PJ. et al., 2015). The authors claim that the inhibition of angiogenesis that we observed following over-expression of MMN2 may depend on the addition of MMRN2 in soluble form that induces the disruption of the interaction complex. On the contrary, in our view, MMRN2 functions as a homeostatic molecule that, once deposited, inhibits the sprouting of new vessels. This hypothesis is supported by the evidence that the molecule is physiologically expressed along all the vessels and it is not likely that once deposited it continues to support vessel sprouting. Thus, an inhibitory role is more probable. In fact, our published observations indicated that down-regulation of the MMRN2 by ECs increased their migration. In addition, here we demonstrated that the down-regulation of MMRN2 expression strongly increased the sprouting of ECs from the spheroids.

On the other end, one cannot exclude that at some stages of EC biology the molecule may exert also a stimulatory function and the different results obtained may depend on the different molecules used to generate the matrix spheroids have been embedded in.

The promising results obtained *in vitro,* prompted us to evaluate the angiostatic function of MMRN2 and its functional deletion mutant *in vivo,* both in normal and in tumor angiogenesis. First, by means of plugs assays, we proved that both molecules strongly inhibited the development of blood vessels. Afterwards, we assessed the role of MMRN2 and its active mutant in tumor-associated angiogenesis. The over-expression of MMRN2 and Δ2 mutant by HT-1080 cells induced a remarkable decrease of tumor growth when injected in nude mice. As previously observed for the whole molecule, we found that the Δ2 deletion mutant did not affect the proliferation or viability of HT-1080 cells in vitro, reinforcing the hypothesis that MMRN2 acts in an indirect way, likely impairing the vascular supply. Accordingly, the *in vivo* analyses carried out by means of the AngioSense® 750EX fluorescent imaging probe indicated that the over-expression of MMRN2 and the Δ2 deletion mutant negatively affected the development of blood vessels within the tumors. These data were corroborated by the analyses of the tumor sections; in fact, the MMRN2 and the Δ2 over-expressing tumors displayed a strong impairment of vascular density suggesting that this effect was responsible for the reduced tumor growth observed. As a consequence, the increased intra-tumoral hypoxia likely induced the expression of HIF-1α, which was particularly high in the Δ2 mutant over-expressing tumors.

In conclusion, taken together these findings provided additional evidences indicating that MMRN2 exerts an angiostatic role. Furthermore in this study we identified the region responsible for the molecular and functional effects of this molecule. The expression of MMRN2 is altered in a wide number of tumor types (Soltermann A. et al., 2008; Shield-Artin KL. et al., 2012; Zanivan S. et al., 2013) and this may significantly affect the development of the intratumoral vasculature. Given the negative role of MMRN2 in the regulation of tumor growth and tumor-associated angiogenesis it cannot be excluded that portions of the molecule may serve to develop potentially novel and powerful anti-angiogenic drugs to be employed for cancer treatment. Given that so far the anti-angiogenic drugs developed have deluded the expectations, there is in fact the need to introduce new more efficacious tools in clinical practice. In this context, the ECM molecule or their matrix-derived fragments (Bellotti D. et al., 2011) are a direct source of angiogenesis regulatory factors and MMRN2 may represent an important tool in this context. Besides the strategy of reducing the blood supply to block cancer growth, in the latest years a new approach has been taking credit. This strategy aims to readdress the aberrant tortuous and leaky vessels associated with the tumor to obtain an efficient vasculature (Sorensen AG. et al., 2012; Emblem KE. et al., 2013; Jain RK. 2014; Wong PP. et al., 2015). This would allow a more efficient delivery of chemotherapy within the tumors and thus a more efficacious treatment.
In this context, there is so far no information as to whether an altered expression of MMRN2 can affect the efficiency of the vessels and vessel homeostasis.

Thus, the second part of my investigation was dedicated to start shed light on this hypothesis and verify if, once deposited, MMRN2 stabilizes the blood vessels counteracting the sprouting of new ones.

First, this aspect was assayed *in vitro* where we observed that MMRN2 is secreted and deposited over time by ECs and that its organization progressively increased until fibrils were formed. Accordingly, our *ex vivo* experiments employing the aortic ring model indicated that, unlike mature vessels, the tip cells of new vessels departing from aortic rings are devoid of MMRN2 (unpublished not shown data) and this likely allows an efficient EC migration to form new blood vessels. Moreover, the analysis of MMRN2 expression in retinal vessels is in agreement with these findings; MMRN2 is almost absent in P1 and P2 stages of retinal development and its expression increases while vessel formation progresses. Interestingly, when the ECs were co-cultured *in vitro* with human pericytes, the deposition of MMRN2 strongly increased and was associated with the formation of a well-defined network of fibrillar structures. This effect was striking strengthened in presence of an increasing percentage of pericytes in co-culture. The mechanism through which pericytes influence ECs, affecting MMRN2 production is still unclear. We are currently evaluating whether this effect requires a direct cell-cell contact between ECs and pericytes or, otherwise, the secretion of specific cytokines by pericytes which may act of ECs to boost MMRN2 secretion and organization.
Not only the pericytes seem to affect MMRN2 expression but also the molecule is a substrate of adhesion for these cells and may also be required for their optimal recruitment, given that MMRN2 knock-out mice display a significant decrease of pericytes' coverage. In this scenario, an initial deposition of MMRN2 by ECs may serve as a substrate for the recruitment and consequent adhesion of pericytes, which, in turn, further boost the expression of the molecule leading to vessel stabilization.

Consistent with a role of MMRN2 as a homeostatic molecule our preliminary results suggest that the glycoprotein stabilizes the EC barrier and plays a role in the proper formation of the ECs' monolayer. In fact, the down-modulation of MMRN2 led to a significant increase of vascular permeability and this was associated with an impaired distribution of the tight junction molecules ZO-1 and OCCLUDIN, whereas VE-cadherin was not affected. It is not yet known how MMRN2 can impinge on the distribution of these molecules and if this depends on the impaired VEGFR2 activation. Given that the expression of the ZO-1 and OCCLUDIN was not altered upon modulation of MMRN2 expression, it is likely that MMRN2 alters the mechanisms thought which the molecules are localized and confined to the tight junctions, possibly perturbing the environment at the EC surface. Interestingly, the molecular alterations seem to reflect on an impaired function not only *in vitro*, but also *in vivo*, since the MMRN2 knock-out mice displayed an increased vascular leakage. Thus, the presence of an efficient endothelial cell barrier seems to require a proper deposition of MMRN2, since its absence was not completely surrogated by other molecules in the murine model.

Taken together, the results presented in this thesis reinforce the angiostatic role of MMRN2 and further dissect the mechanisms involved. Furthermore, we identified the region of the molecule responsible for these effects and provide preliminary evidences indicating that MMRN2 may function as a 'biological barrier' keeping ECs in a steady-state and stabilizing the vasculature.

In conclusion, these results spur us to further shed light on the intricate mechanisms through which MMRN2 affects vessels' homeostasis, thus representing a crucial molecule for the maintenance of blood vessel integrity.

.

8. REFERENCES

Adam F, Zheng S, Joshi N, Kelton DS, Sandhu A, Suehiro Y, Jeimy SB, Santos AV, Massé JM, Kelton JG, Cramer EM, Hayward CP. Analyses of cellular multimerin 1 receptors: in vitro evidence of binding mediated by alphaIIbbeta3 and alphavbeta3. *Thromb Haemost*. 2005 94(5):1004-11.

Aghajanian A, Wittchen E.S, Allingham M.J, Garrett T.A, and Burridge K. Endothelial cell junctions and the regulation of vascular permeability and leukocyte transmigration. *J Thromb Haemost* 2008 Sep; 6(9): 1453-1460

Amma LL, Goodyear R, Faris JS, Jones I, Ng L, Richardson G, Forrest D. An emilin family extracellular matrix protein identified in the cochlear basilar membrane. *Mol Cell Neurosci* 2003 23(3):460-72.

Aonuma M, Saeki Y, Akimoto T, Nakayama Y, Hattori C, Yoshitake Y, Nishikawa K, Shibuya M, Tanaka N. G. Vascular endothelial growth factor overproduced by tumour cells acts predominantly as a potent angiogenic factor contributing to malignant progression. *Int. J. Exp. Pathol*., 80*:* 271-281, 1999.

Aviezer D, Hecht D, Safran M, Eisinger M, David G, and Yayon A. Perlecan, basal lamina proteoglycan, promotes basic fibroblast growth factor-receptor binding, mitogenesis, and angiogenesis. *Cell.* 1994; 79: 1005-1013.

Balbay MD, Pettaway CA, Kuniyasu H, Inoue K, Ramirez E, Li E, Fidler IJ, Dinney CP. Highly metastatic human prostate cancer growing within the prostate of athymic mice over expresses vascular endothelial growth factor. *Clin Cancer Res.* 1999 Apr;5(4):783-9.

Baldwin ME, Roufail S, Halford MM, Alitalo K, Stacker SA, Achen MG. Multiple forms of mouse vascular endothelial growth factor-D are generated by RNA splicing and proteolysis. *J Biol Chem.* 2001 Nov 23;276(47):44307-14.

Beese M, Wyss K, Haubitz M, Kirsch T. Effect of cAMP derivates on assembly and maintenance of tight junctions in human umbilical veinendothelial cells. *BMC Cell Biol.* 2010 Sep 7;11:68.

Belotti D, Foglieni C, Resovi A, Giavazzi R, Taraboletti G. Targeting angiogenesis with compounds from the extracellular matrix. *Int J Biochem Cell Biol*. 2011 43(12):1674-85.

Bergers G, Benjamin LE. Tumorigenesis and the angiogenic switch. *Nat Rev Cancer*.2003 Jun; 3(6):401-10.

Bergers G, Steven Song. The role of pericytes in blood-vessel formation and maintenance. *Neuro Oncol.* 2005 Oct; 7(4): 452–464.

Bissell MJ, Kenny PA, Radisky DC. Microenvironmental regulators of tissue structure and function also regulate tumor induction and progression: the role of extracellular matrix and its degrading enzymes. *Cold Spring Harb Symp Quant Biol*. 2005 70:343-56.

Braghetta P, Ferrari A, De Gemmis P, Zanetti M, Volpin D, Bonaldo P, Bressan GM. Expression of the EMILIN-1 gene during mouse development. *Matrix Biol*. 2002 21(7):603-9.

Braghetta P, **Ferrari A, De Gemmis P, Zanetti M, Volpin D, Bonaldo P, Bressan GM.** Overlapping, complementary and site-specific expression pattern of genes of the EMILIN/Multimerin family. *Matrix Biol*. 2004 22(7): 549-56.

Bressan GM, Daga-Gordini D, Colombatti A, Castellani I, Marigo V, Volpin D. Emilin, a component of elastic fibers preferentially located at the elastinmicrofibrils interface *J Cell Biol* 1993 121(1):201-12.

Bryan BA, Walshe TE, Mitchell DC, Havumaki JS, Saint-Geniez M, Maharaj AS, Maldonado AE, D'Amore PA. Coordinated vascular endothelial growth factor expression and signaling during skeletal myogenic differentiation. *Mol Biol Cell*. 2008 Mar;19(3):994-1006.

Carmeliet P, Lampugnani MG, Moons L, Breviario F, Compernolle V, Bono F, Balconi G, Spagnuolo R, Oosthuyse B, Dewerchin M, Zanetti A, Angellilo A, Mattot V, Nuyens D, Lutgens E, Clotman F, de Ruiter MC, Gittenberger-de Groot A, Poelmann R, Lupu F, Herbert JM, Collen D, Dejana E. Targeted deficiency or cytosolic truncation of the VE-cadherin gene in mice impairs VEGF-mediated endothelial survival and angiogenesis. *Cell.* 1999 Jul 23;98(2):147-57.

Carmeliet P. Mechanisms of angiogenesis and arteriogenesis. *Nat Med*. 2000; 6:389 –395.

Carmeliet P, Jain RK. Molecular mechanisms and clinical applications of angiogenesis. *Nature.* 2011; 473: 298–307.

Carmeliet P. Blood vessels and nerves: common signals, pathways and diseases. *Nat Rev Genet.* 2003; 4(9):710-20.

Cascone T, Heymach JV. Targeting the angiopoietin/Tie2 pathway: cutting tumor vessels with a double-edged sword? *J Clin Oncol*. 2012; 30: 441–444.

Cheresh DA, Stupack DG. Regulation of angiogenesis: apoptotic cues from the ECM. *Oncogene.* 2008; 27: 6285-6298.

Chiodelli P, Bugatti A, Urbinati C, and Rusnati M. Heparin/ Heparan sulfate proteoglycans glycomic interactome in angiogenesis: biological implications and therapeutical use. *Molecules.* 2015; 20: 6342–6388.

Christian S., Ahorn H., Novatchkova M., Garin-Chesa P., Park J.E., Weber G., Eisenhaber F., Rettig W.J., Lenter M.C. Molecular cloning and characterization of EndoGlyx-1, an EMILIN-like multisubunit glycoprotein of vascular endothelium. *J Biol Chem* 2001 276(51):48588-95.

Colladel R., Pellicani R., Andreuzzi E., Paulitti A., Tarticchio G., Todaro F., Colombatti F., Mongiat M. MULTIMERIN2 binds VEGF-A primarily via the carbohydrate chains exerting an angiostatic function and impairing tumor growth. *Oncotarget* 2015 Dec 9. Dooi: 10.18632

Colombatti A, **Bressan GM, Castellani I, Volpin D.** Glycoprotein 115, a glycoprotein isolated from chick blood vessels, is widely distributed in connective tissue. *J Cell Biol* 1985 100(1):18-26.

Colombatti A, Spessotto P, Doliana R, Mongiat M, Bressan GM, Esposito G. The EMILIN/Multimerin family. *Front Immunol.* 2011;2:93.

Crosby CV, Fleming PA, Argraves WS, Corada M, Zanetta L, Dejana E, Drake CJ. VE-cadherin is not required for the formation of nascent blood vessels but acts to prevent their disassembly. *Blood.* 2005 Apr 1;105(7):2771-6.

Danussi C., Spessotto P., Petrucco A., Wassermann B., Sabatelli P., Montesi M., Doliana R., Bressan G.M., Colombatti A. Emilin1 deficiency causes structural and functional defects of lymphatic vasculature. *Mol. Cell. Biol*. 2008 28:4026–4039.

Danussi C, Petrucco A, Wassermann B, Modica TM, Pivetta E, Del Bel Belluz L, Colombatti A, Spessotto P. An EMILIN1-negative microenvironment promotes tumor cell proliferation and lymph node invasion. *Cancer Prev Res.* 2012 Sep;5(9):1131-43.

Davis GE, Pintar Allen KA, Salazar R, Maxwell SA. Matrix metalloproteinase -1 and -9 activation by plasmin regulates a novel endothelial cell mediated mechanism of collagen gel contraction and capillary tube regression in three-dimensional collagen matrices. *J Cell Sci.* 2001 Mar;114(Pt 5):917-30.

Dejana, E. Endothelial cell-cell junctions: happy together. *Nat Rev Mol Cell Biol*. 2004 ;5(4):261-70.

De Vita V., Lawrence T., Rosenberg S. Cancer principles and practice of oncology 2007 e-book, 7th edition. Dhanabal.

Doliana R, Bot S, Bonaldo P, Colombatti A. EMI, a novel cysteine-rich domain of EMILINs and other extracellular proteins, interacts with the gC1q domains and participates in multimerization. *FEBS Lett* 2000 484(2): 164-8.

Doliana R, Bot S, Mungiguerra G, Canton A, Cilli SP, Colombatti A. Isolation and Characterization of EMILIN-2, a New Component of the Growing EMILINs Family and a Member of the EMI Domain containing Superfamily. *J Biol Chem*. 2001 276(15): 12003-11.

Ebos JM, Lee CR, Cruz-Munoz W, Bjarnason GA, Christensen JG, and Kerbel RS. Accelerated metastasis after short-term treatment with a potent inhibitor of tumor angiogenesis. *Cancer Cell.* 2009; 15: 232–239.

Emblem KE, Mouridsen K, Bjornerud A, Farrar CT, Jennings D, Borra RJ, Wen PY, Ivy P, Batchelor TT, Rosen BR, Jain RK, Sorensen AG. Vessel architectural imaging identifies cancer patient responders to anti-angiogenic therapy. *Nat Med.* 2013 Sep;19(9):1178-83.

Ferrara N. VEGF as a therapeutic target in cancer. *Oncology.* 2005; 69 Suppl 3: 11–16.

Folkman J. Tumor angiogenesis: therapeutic implications *N Eng J Med* 1971 285:1182-1186.

Garcia JG, Davis HW, Patterson CE. Regulation of endothelial cell gap formation and barrier dysfunction: role of myosin light chain phosphorylation. *J Cell Physiol.* 1995 Jun;163(3):510-22.

Gavard, J. Breaking the VE-cadherin bonds. *FEBS Lett.(*2009) Jan 5;583(1):1-6.

Goeckeler ZM, Wysolmerski RB. Myosin light chain kinase-regulated endothelial cell contraction: the relationship between isometric tension, actin polymerization, and myosin phosphorylation. *J Cell Biol*. 1995;130: 613–627.

Goishi K, Klagsbrun M. Vascular endothelial growth factor and its receptors in embryonic zebrafish blood vessel development. *Curr Top Dev Biol.* 2004 62:127–152.

Hayward CP, Warkentin TE, Horsewood P, Kelton JG. Multimerin: a series of large disulfide-linked multimeric proteins within platelets *Blood* 1991 77(12):2556-60.

Hayward CP. Multimerin: a bench-to-bedside chronology of a unique platelet and endothelial cell protein--from discovery to function to abnormalities in disease. *Clin Invest Med*. 1997 20(3):176-87.

Hanahan D, Folkman J. Patterns and emerging mechanisms of the angiogenic switch during tumorigenesis. *Cell*. 1996 86(3):353-64.

Hileman RE, Fromm JR, Weiler JM, Linhardt RJ. Glycosaminoglycan-protein interactions: definition of consensus sites in glycosaminoglycan binding proteins. *Bioessays* 1998 20(2):156-67.

Hirase T, Staddon JM, Saitou M, Ando-Akatsuka Y, Itoh M, Furuse M, Fujimoto K, Tsukita S, Rubin LL. Occludin as a possible determinant of tight junction permeability in endothelial cells. *J Cell Sci*. 1997 Jul;110 (Pt 14):1603-13.

Ingber DE, Folkman J. How does extracellular matrix control capillary morphogenesis? Cell. 1989; 58: 803-805.

Jaffe EA, Nachman RL, Becker CG, and Minick CR. Culture of human endothelial cells derived from umbilical veins. Identification by morphologic and immunologic criteria. *J Clin Invest.* 1973; 52: 2745–2756.

Jain RK. Normalization of tumor vasculature: an emerging concept in antiangiogenic therapy. *Science.* 2005 Jan 7;307(5706):58-62.

Jain RK. Antiangiogenesis strategies revisited: from starving tumors to alleviating hypoxia. *Cancer Cell.* 2014 Nov 10;26(5):605-22.

Järveläinen H, Sainio A, Koulu M, Wight TN, Penttinen R. Extracellular matrix molecules: potential targets in pharmacotherapy. *Pharmacol Rev.* 2009 Jun;61(2):198-223.

Jarvelainen H, Sainio A, and Wight TN. Pivotal role for decorin in angiogenesis. Matrix Biol. 2015; 43: 15-26.

Jeimy SB, Fuller N, Tasneem S, Segers K, Stafford AR, Weitz JI, Camire RM, Nicolaes GA, Hayward CP. Multimerin 1 binds factor V and activated factor V with high affinity and inhibits thrombin generation. *Thromb Haemost*. 2008 100(6):1058-67.

Jendraschak E, Helene Sage E. Regulation of angiogenesis by SPARC and angiostatin: implications for tumor cell biology. *Semin Cancer Biol.* 1996; 7: 139-146.

Jin K, Mao XO,Greenberg DA. Vascular endothelial growth factor stimulates neurite outgrowth from cerebral cortical neurons via Rho kinase signaling. *J Neurobiol.* 2006 Feb 15;66(3):236-42.

Kang K, Lim JS. Induction of functional changes of dendritic cells by silica nanoparticles. *Immune Netw*. 2012; 12: 104–112.

Kitamura M, Toi M, Arai K, Iwasaki Y, Suzuki H, Matsuo K. Concentrations of vascular endothelial growth factor in the sera of gastric cancer patients. *Oncol Rep*. 1998 Nov-Dec; 5(6):1419-24.

Kurebayashi J, Otsuki T, Kunisue H, Mikami Y, Tanaka K, Yamamoto S, Sonoo H. Expression of vascular endothelial growth factor (VEGF) family members in breast cancer. *Jpn J Cancer Res.* 1999 Sep;90(9):977-81.

Lamalice L, Houle F, Jourdan G, Huot J. Phosphorylation of tyrosine 1214 on VEGFR2 is required for VEGF-induced activation of Cdc42 upstream of SAPK2/p38. *Oncogene*. 2004 15;23(2):434-45.

Lawler PR, Lawler J. Molecular Basis for the Regulation of Angiogenesis by Thrombospondin-1 and -2. *Cold Spring Harb Perspect Med.* 2012; 2.

LeBleu V.S., MacDonald B. and Kalluri R. Structure and Function of Basement Membranes. *Experimental Biology and Medicine* 2007 232:1121-1129.

Lee JS, Gotlieb AI. Microtubules regulate aortic endothelial cell actin microfilament reorganization in intact and repairing monolayers. *Histol Histopathol* 2005 20: 455–465.

Leimeister C., Steidl C., Schumacher N., Erhard S., Gessler M. Developmental expression and biochemical characterization of Emu family members *Dev Biol* 2002 249: 204–218.

Li R, Luo M, Ren M, Chen N, Xia J, Deng X, Zeng M, Yan K, Luo T, and Wu J. Vitronectin Regulation of Vascular Endothelial Growth Factor-Mediated Angiogenesis. *J Vasc Res.* 2014; 51: 110-117.

Lorenzon E, Colladel R, Andreuzzi E, Marastoni S, Todaro F, Schiappacassi M, Ligresti G, Colombatti A, Mongiat M. MULTIMERIN2 impairs tumor angiogenesis and growth by interfering with VEGF-A/VEGFR2 pathway. Oncogene. 2012 Jun 28;31(26):3136-47.

Mammoto T, Jiang A, Jiang E, Panigrahy D, Kieran MW, and Mammoto A. Role of Collagen Matrix in Tumor Angiogenesis and Glioblastoma Multiforme Progression. *Am J Pathol.* 2013; 183: 1293-1305.

Manickam V, Tiwari A, Jung JJ, Bhattacharya R, Goel A, Mukhopadhyay D, and Choudhury A. Regulation of vascular endothelial growth factor receptor 2 trafficking and angiogenesis by Golgi localized t-SNARE syntaxin 6. *Blood.* 2011; 117: 1425–1435.

Marastoni S, Andreuzzi E, Paulitti A, Colladel R, Pellicani R, Todaro F, Schiavinato A, Bonaldo P, Colombatti A, Mongiat M. EMILIN2 down-modulates the Wnt signalling pathway and suppresses breast cancer cell growth and migration. *J Pathol.*2014 Mar;232(4):391-404.

Mongiat M., Mungiguerra G., Bot S., Mucignat M.T., Giacomello E., Doliana R., Colombatti A. Self-assembly and supramolecular organization of EMILIN. *J Biol Chem* 2000 275(33): 25471-25480.

Mongiat M., Ligresti G., Marastoni S., Lorenzon E., Doliana R., Colombatti A. Regulation of the extrinsic apoptotic pathway by the extracellular matrix glycoprotein EMILIN2 *Mol Cell Biol* 2007 27: 7176-7187.

Mongiat M, Marastoni S, Ligresti G, Lorenzon E, Schiappacassi M, Perris R, Frustaci S, and Colombatti A. The extracellular matrix glycoprotein elastin microfibril interface located protein 2: a dual role in the tumor microenvironment. *Neoplasia*. 2010 12: 294-304.

Nagy JA, Chang SH, Dvorak AM, Dvorak HF. Why are tumour blood vessels abnormal and why is it important to know? *Br J Cancer.* 2009 Mar 24;100(6):865-9.

Nakatsu MN, Davis J, and Hughes CC. Optimized fibrin gel bead assay for the study of angiogenesis. *J Vis Exp*. 2007186.

Neve A, Cantatore FP, Maruotti N, Corrado A, and Ribatti D. Extracellular matrix modulates angiogenesis in physiological and pathological conditions. *Biomed Res Int.* 2014; 2014: 756078.

Noy PJ, Lodhia P, Khan K, Zhuang X, Ward DG, Verissimo AR, Bacon A, and Bicknell R. Blocking CLEC14A-MMRN2 binding inhibits sprouting angiogenesis and tumour growth. *Oncogene.* 2015.

Olsson AK, Dimberg A, Kreuger J, Claesson-Welsh L. VEGF receptor signaling in control of vascular function. *Nat Rev Mol Cell Biol* 2006 7: 359–371.

Papetti, M. and Herman, I.M. Mechanisms of normal and tumour-derived angiogenesis. *Am. J.Physiol. Cell Physiol.* 2002 282, C947–C970.

Pepper MS. Extracellular proteolysis and angiogenesis. *Thromb Haemost*. 2001 86(1):346-55.

Pitulescu ME, Schmidt I, Benedito R, Adams RH. Inducible gene targeting in the neonatal vasculature and analysis of retinal angiogenesis in mice. *Nat Protc.*2010 Sep;5(9):1518-34.

Risau, W. Mechanisms of angiogenesis. *Nature* 1997; 386: 671– 674.

Risau W, Flamme I. Vasculogenesis. *Annu Rev Cell Dev Biol.* 1995. 11:73–91.

Rozario T, DeSimone DW. The extracellular matrix in development and morphogenesis: a dynamic view. *Dev Biol.* 2010 May 1;341(1):126-40.

Sanz-Moncasi MP, Garin-Chesa P, Stockert E, Jaffe EA, Old LJ, Rettig WJ. Identification of a high molecular weight endothelial cell surface glycoprotein, endoGlyx-1, in normal and tumor blood vessels *Lab Invest* 1994 71(3):366-73.

Schiavinato A, Becker AK, Zanetti M, Corallo D, Milanetto M, Bizzotto D, Bressan G, Guljelmovic M, Paulsson M, Wagener R, Braghetta P, Bonaldo P. EMILIN-3, peculiar member of elastin microfibril interface-located protein (EMILIN) family, has distinct expression pattern, forms oligomeric assemblies, and serves as transforming growth factor β (TGF-β) antagonist. *J Biol Chem*. 2012 287(14):11498-515.

Shield-Artin KL, Bailey MJ, Oliva K, Liovic AK, Barker G, Dellios NL, Reisman S, Ayhan M, and Rice GE. Identification of ovarian cancer-associated proteins in symptomatic women: a novel method for semi-quantitative plasma proteomics. *Proteomics Clin Appl.* 2012n/a.

Senger DR, Davis GE. Angiogenesis. *Cold Spring Harb Perspect Biol*. 2011; 3: a005090.

Seo Y, Baba H, Fukuda T, Takashima M, Sugimachi K. High expression of vascular endothelial growth factor is associated with liver metastasis and a poor prognosis for patients with ductal pancreatic adenocarcinoma. *Cancer.* 2000 May 15;88(10):2239-45.

Shasby DM, Shasby SS, Sullivan JM, Peach MJ. Role of endothelial cell cytoskeleton in control of endothelial permeability. *Circ Res* 1982 51:657–661.

Shaheen RM, Davis DW, Liu W, Zebrowski BK, Wilson MR, Bucana CD, McConkey DJ, McMahon G, Ellis LM. Antiangiogenic therapy targeting the tyrosine kinase receptor for vascular endothelial growth factor receptor inhibits the growth of colon cancer liver metastasis and induces tumor and endothelial cell apoptosis. *Cancer Res.* 1999 Nov 1;59(21):5412-6.

Shasby DM, Shasby SS, Sullivan JM, Peach MJ. Role of endothelial cell cytoskeleton in control of endothelial permeability. *Circ Res.* 1982 51: 657–661.

Shen Q, Rigor RR, Pivetti CD, Wu MH, Yuan SY. Myosin light chain kinase in microvascular endothelial barrier function. *Cardiovasc Res*.2010 Jul 15;87(2):272-80. doi: 10.1093/cvr/cvq144.

Shen Q, Wu MH, Yuan SY. Endothelial contractile cytoskeleton and microvascular permeability. *Cell Health Cytoskelet.* 2009 Jul 1;2009(1):43-50.

Simon-Assmann P, Orend G, Mammadova-Bach E, Spenle C, and Lefebvre O. Role of laminins in physiological and pathological angiogenesis. *Int J Dev Biol.* 2011; 55: 455-465.

Sobel M, Soler DF, Kermode JC, Harris RB. Localization and characterization of a heparin binding domain peptide of human von Willebrand factor. *J Biol Chem*. 1992 267(13):8857-62.

Soltermann A, Ossola R, Kilgus-Hawelski S, von EA, Suter T, Aebersold R, and Moch H. N-glycoprotein profiling of lung adenocarcinoma pleural effusions by shotgun proteomics. *Cancer. 2008; 114: 124–133.*

Sorensen AG, Emblem KE, Polaskova P, Jennings D, Kim H, Ancukiewicz M, Wang M, Wen PY, Ivy P, Batchelor TT, and Jain RK. Increased survival of glioblastoma patients who respond to antiangiogenic therapy with elevated blood perfusion. *Cancer Res*. 2012; 72: 402–407.

Spessotto P, **Cervi M, Mucignat MT, Mungiguerra G, Sartoretto I, Doliana R, Colombatti A.** Beta 1 Integrin-dependent cell adhesion to EMILIN-1 is mediated by the gC1q domain. *J Biol Chem*. 2003 278(8): 6160-7.

Sternlicht MD,Werb Z. How matrix metalloproteinases regulate cell behavior. *Annu Rev Cell Dev Biol.* 2001;17:463-516.

Sullivan LA, Brekken RA. The VEGF family in cancer and antibody-based strategies for their inhibition. *MAbs.* 2010 Mar-Apr;2(2):165-75.

Takahashi T, Yamaguchi S, Chida K, Shibuya M. A single autophosphorylation site on KDR/Flk-1 is essential for VEGF-A-dependent activation of PLC-gamma and DNA synthesis in vascular endothelial cells. *EMBO J.* 2001 20(11):2768-78.

Totsukawa G, Yamakita Y, Yamashiro S, Hartshorne DJ, Sasaki Y, Matsumura F. Distinct roles of ROCK (Rho kinase)and MLCK in spatial regulation of MLC phosphorylation for assembly of stress fibers and focal adhesions in 3T3 fibroblasts. *J Cell Biol.* 2000 Aug 21;150(4):797-806.

Vempati P, Popel AS, and Mac GF. Extracellular regulation of VEGF: isoforms, proteolysis, and vascular patterning. *Cytokine Growth Factor Rev*. 2014; 25: 1–19.

Verin AD, Patterson CE, Day MA, Garcia JG. Regulation of endothelial cell gap formation and barrier function by myosin associated phosphatase activities. *Am J Physiol*. 1995 Jul;269(1Pt 1):L99-108.

Wong PP, Demircioglu F, Ghazaly E, Alrawashdeh W, Stratford MR, Scudamore CL, Cereser B, Crnogorac-Jurcevic T, McDonald S, Elia G, Hagemann T, Kocher HM, Hodivala-Dilke KM. Dual-action combination therapy enhances angiogenesis while reducing tumor growth and spread. *Cancer Cell.* 2015 Jan 12;27(1):123-37.

Yi M, Ruoslahti E. A fibronectin fragment inhibits tumor growth, angiogenesis, and metastasis. *Proc Natl Acad Sci*. 2001; 98: 620-624.

Yoshiji H1, Kuriyama S, Hicklin DJ, Huber J, Yoshii J, Ikenaka Y, Noguchi R, Nakatani T, Tsujinoue H, Fukui H. The vascular endothelial growth factor receptor KDR/Flk-1 is a major regulator of malignant ascites formation in the mouse hepatocellular carcinoma model. *Hepatology*. 2001 Apr;33(4):841-7.

Yuan SY, Rigor RR. Regulation of Endothelial Barrier Function. San Rafael (CA): Morgan & Claypool Life Sciences; 2010.

Zanivan S, Maione F, Hein MY, Hernandez-Fernaud JR, Ostasiewicz P, Giraudo E, and Mann M. SILAC-Based Proteomics of Human Primary Endothelial Cell Morphogenesis Unveils Tumor Angiogenic Markers. *Mol Cell Proteomics*. 2013; 12: 3599–3611.

9. PUBLICATIONS

Roberta Colladel, Rosanna Pellicani, Eva Andreuzzi, Alice Paulitti, Giulia Tarticchio, Federico Todaro, Alfonso Colombatti, Maurizio Mongiat. MULTIMERIN2 binds VEGF-A primarily via the carbohydrate chains exerting an angiostatic function and impairing tumor growth. *Oncotarget* 2015 Dec 9. Dooi: 10.18632.

Stefano Marastoni, Eva Andreuzzi, Alice Paulitti, Roberta Colladel, Rosanna Pellicani, Federico Todaro, Alvise Schiavinato, Paolo Bonaldo, Alfonso Colombatti and Maurizio Mongiat. EMILIN2 down-modulates the Wnt Signalling pathway and suppresses breast cancer cell growth and migration. *J. Pathol.* 2014 Mar; 232(4):391-404.

Silvestri A, Pin E, Huijbers A, Pellicani R, Parasido EM, Pierobon M, Petricoin E, Liotta L, Belluco C. Individualized therapy for metastatic colorectal cancer. J Intern Med. 2013 Jul;274(1):1-24.

ACKNOWLEDGMENTS

This work was performed in the Division of Experimental Oncology 2 at
National Cancer Institute (CRO) of Aviano.

I would like to acknowledge the “Tumor microenvironment and Angiogenesis”
group, in particular my PhD advisor, Dr. Maurizio Mongiat
for supporting me during these years.